Journal of Controlled Release 356 (2023) 26–42

Contents lists available at ScienceDirect

Journal of Controlled Release

journal homepage: www.elsevier.com/locate/jconrel

Single-chain polymer nanoparticles in biomedical applications

Naomi M. Hamelmann, Jos M.J. Paulusse *

Department of Molecules and Materials, MESA+ Institute for Nanotechnology and TechMed Institute for Health and Biomedical Technologies, Faculty of Science and Technology, University of Twente, P.O. Box 217, 7500 AE Enschede, the Netherlands

ARTICLE INFO

Keywords:
Single chain polymer nanoparticles
Biomedical applications
Targeted imaging
Controlled drug delivery
Antimicrobial

ABSTRACT

Single-chain polymer nanoparticles (SCNPs) are a well-defined and uniquely sized class of polymer nanoparticles. The advances in polymer science over the past decades have enabled the development of a variety of intramolecular crosslinking systems, leading to particles in the 5–20 nm size regime. Which is aligned with the size regime of proteins and therefore making SCNPs an interesting class of NPs for biomedical applications. The high modularity of SCNP design and the ease of their functionalization have led to growing research interest. In this review, we describe different crosslinking systems, as well as the preparation of functional SCNPs and the variety of biomedical applications that have been explored.

1. Introduction

Nanomedicine provides the opportunity to transport therapeutics and imaging agents largely irrespective of their physicochemical properties to specific tissues for an enhanced mode of action. Polymer nanoparticles (NPs) provide the ability to readily adapt their surface chemistry, as well as the composition and size of the nanocarriers. Single-chain polymer nanoparticles are a well-defined class of nanocarriers that are prepared by intramolecular crosslinking of individual polymer chains. As a result, particle size is highly dependent on the precursor polymer, which can be readily prepared utilizing controlled/living polymerization techniques [1,2], and have been demonstrated to form monodisperse particles as small as 5–20 nm. SCNP formation has been achieved both via supramolecular and covalent crosslinking, yielding dynamic as well as irreversible nanoparticle systems. A wide variety of synthetic strategies has been employed in the crosslinking reaction including homo- [3,4] and hetero-coupling [5,6] of monomer units as well as crosslinker induced chain folding [7–9]. SCNP size is typically in the range of proteins, and is dependent on the length of the precursor polymer [10] and crosslinking density [11]. Kröger et al. have shown an decrease in hydrodynamic volume for polymer to SCNP from 90 to 30 kDa [10]. Furthermore, the formation of SCNPs has analogies with the folding observed for proteins, which has great potential in biomedical applications including protein and enzyme mimicry [12,13]. Polymer chemistry provides a virtually unlimited diversity for the preparation of functional SCNPs, providing water solubility, biocompatibility and targeting capabilities by controlling the surface chemistry of the particles. The synthesis of SCNPs is monitored by a variety of characterization techniques, including size exclusion chromatography (SEC) to analyze chain collapse in SCNPs, NMR spectroscopy for evaluation of the chemical structure, while size measurements are typically carried out by dynamic light scattering (DLS), atomic force microscopy (AFM), small angle x-ray scattering (SAXS) and transmission electron microscopy (TEM) [14–16].

Over the past few years, increasing research effort has been focused towards application-based SCNPs. This includes cell targeting and controlling the subcellular location of SCNPs. Further, drug encapsulation and release profiles of SCNP nanocarriers have been investigated for controlled drug delivery applications [17–19]. SCNPs have furthermore shown interesting characteristics in anti-bacterial applications [20,21]. Incorporation of imaging agents in SCNPs has been explored, for example through integration of the imaging modality in the employed crosslinker [9]. Considering the size of SCNPs resembling that of proteins and small viruses, mimicking of enzymes and proteins is an appealing research goal [22,23]. Folding processes in SCNPs are, for example, being explored by introducing sequential crosslinking [24,25], but also the integration of catalysts inside SCNPs has been investigated for improved catalyst stability and recyclability [26]. Earlier reviews have focused on the formation [27–29] and characterization [16] of SCNPs. In this review, a brief overview on SCNP synthesis and functionalization is given, while discussing in detail cellular interactions with SCNPs and their biomedical applications.

* Corresponding author.
E-mail address: j.m.j.Paulusse@utwente.nl (J.M.J. Paulusse).

https://doi.org/10.1016/j.jconrel.2023.02.019
Received 1 September 2022; Received in revised form 2 January 2023; Accepted 13 February 2023
Available online 1 March 2023

2. SCNP crosslinking

Many crosslinking strategies have been developed to obtain SCNPs that are exclusively intramolecularly crosslinked, excluding the formation of nanoparticles consisting of multiple polymer chains. These strategies include covalent crosslinking [8,25,30,31], supramolecular interactions [32,33] and metal complexation (see Fig. 1) [34].

2.1. Covalent crosslinking

One of the earliest developed SCNP systems is based on a coupling reaction of benzocyclobutene units, which dimerize at elevated temperatures (i.e. 250 °C in dibenzyl ether) [30,35]. Milder synthesis routes have been explored, such as amidation reactions [36] and urea formation [11], which can be carried out at ambient temperature. Although initially most SCNP crosslinking processes were carried out in organic solvent [36], many crosslinking approaches can now also be carried out in aqueous solution [37–39]. Thiol-functional monomers have been used in thiol-Michael reactions with a diacrylate crosslinker to yield covalently crosslinked SCNPs [8,10,40]. This strategy was adapted for various functional *co*-polymers, both in organic solvent, as well as in water. Garcia and coworkers prepared SCNPs from the natural polymer dextran. Dextran was functionalized with methacrylate groups, which were subsequently crosslinked via thiol-Michael addition with a dithiol crosslinker [7,41]. A different type of bifunctional crosslinker is 1,4-diiodobutane, which was used to quaternize tertiary amines in poly(*N*,*N*-dimethylamino)ethyl methacrylate [42], as well as in crosslinking through nucleophilic substitution [21,43]. Click chemistry has been utilized either with two complementary functional monomers [44] or with the introduction of a crosslinker [31,45,46]. Crosslinkers with additional functionalities including the binding of contrast agents or radiolabels for imaging have been introduced by click chemistry as well [9,37]. More recently, interest in light induced crosslinking has increased. Since the first reports on crosslinking of maleimide (Mal) and tetrazole (Tet) moieties resulting in nitrile imine-mediated tetrazole-ene cycloaddition (NITEC) [5,47–49] the body of work has grown considerably with a variety of light-activated complementary monomers [3,25,50].

2.2. Dynamic covalent crosslinking

Degradable NPs have shown important advantages in controlled drug delivery, both to ensure biocompatibility, but also to release drugs in response to a trigger [51]. Several strategies to incorporate responsiveness in SCNPs have been studied, such as pH [33,36], temperature [6,50] and UV irradiation [52]. An interesting example of responsive SCNPs is based on a polymer including 2-(acetoacetoxy)ethyl methacrylate, which was functionalized with a monofunctional enamine to enable exchange with ethylenediamine [36]. This reaction was used to crosslink SCNPs covalently and enamine bond rupture was shown to be induced under acidic conditions, as determined by ^{1}H NMR spectroscopy. This class of SCNPs displays spontaneous formation of enamines and exchange with the bifunctional crosslinker, while they can also be degraded by hydrolysis. Dynamic disulfide crosslinking was utilized by Song et al., who employed a precursor polymer consisting of hydroxyethyl methacrylate (HEMA) and pyridyldisulfide ethyl methacrylate (PDSEMA) [53]. The PDSEMA block was deprotected to obtain free thiols which formed intramolecular crosslinks via disulfide bridges under high dilutions. In this work, Nile red was encapsulated and the release was studied via redox stimuli. DTT was incubated with the SCNPs at increasing concentrations, showing only minor release at 5 μM DTT and a strong burst release at 5 mM DTT. Addition of DTT resulted in cleavage of disulfide bonds in the SCNPs and returned the SCNPs back to their polymer form. Photodegradability is another strategy investigated to improve the breakdown of SCNPs. Polyesters bearing UV-active coumarin units in the polymer backbone were synthesized by Fan and coworkers [52]. The polymer was crosslinked by photodimerization of the coumarin units under UV irradiation at 320 nm, and the degradation by photocleavage was demonstrated upon UV radiation at 254 nm, which resulted in chain scission. Enzyme based degradation of SCNPs was investigated by Offenloch and co-workers [48]. An acyclic diene metathesis (ADMET) polymerization was utilized to form a self-immolative polymer with functional side groups for photoactivated crosslinking. The intramolecular crosslinking of the Tet and Mal functional groups was induced under UV irradiation at 320 nm. As earlier described [54], degradation of the main chain was achieved in the presence of $Na_2S_2O_4$, which mimics the azoreductase enzyme present in cells. As most polymers used for SCNP formation are prepared via radical polymerization, their backbone consists of carbon-carbon bonds, which are difficult to degrade. Radical ring opening polymerization of cyclic vinyl monomers is an elegant strategy to render vinyl polymers degradable [55]. SCNPs with main chain degradability were prepared from *co*-polymers containing 2-methylene-1,3-dioxepane (MDO) and an NHS-ester functional monomer, which was crosslinked with diamines (see Fig. 2) [56]. The main chain was demonstrated to degrade via ester hydrolysis of the ring opened MDO monomer in the polymer backbone.

2.3. Supramolecular crosslinking

Supramolecular crosslinking via hydrogen bonding has been employed in various SCNP systems built on benzamides [57], benzene-1,3,5-tricarboxamides (BTA) [12,22,58–61], urea [62], 2-ureido-4[1H]-

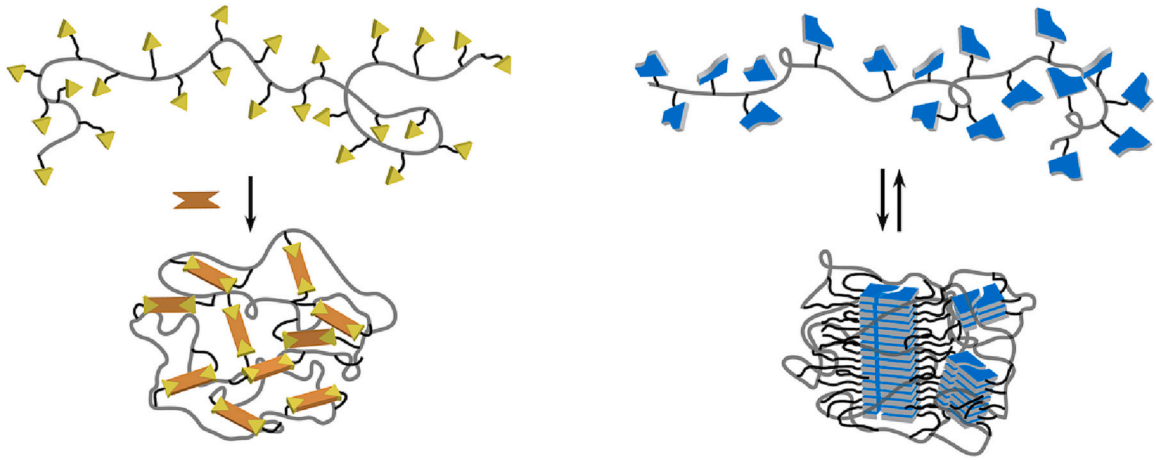

Fig. 1. Illustration of crosslinking strategies including crosslinker induced crosslinking (left) and supramolecular crosslinking (right).

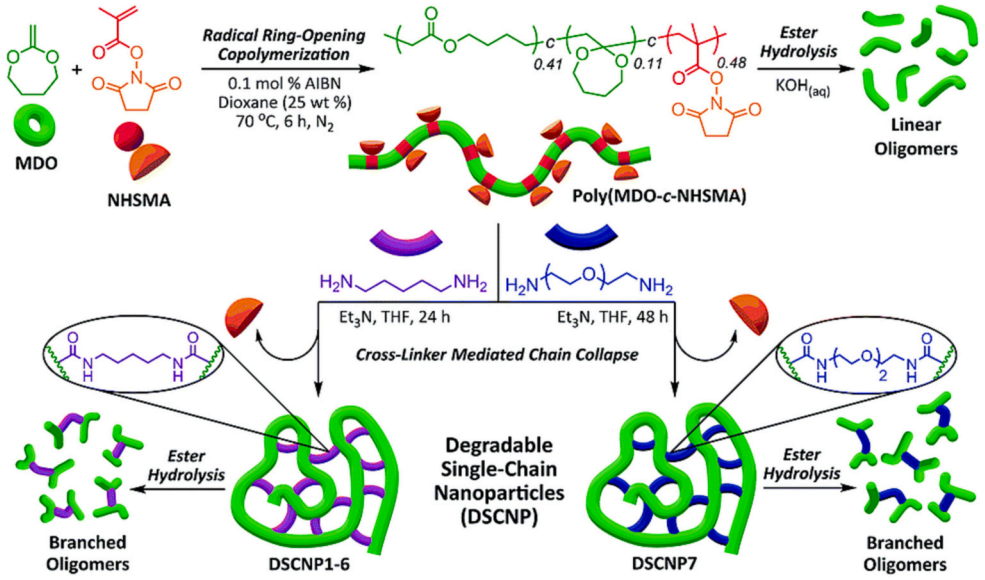

Fig. 2. Schematic presentation of polymer synthesis via radical ring-opening *co*-polymerization, SCNP formation utilizing diamine crosslinker and degradation via ester hydrolysis. Reproduced with permission from ref. [56] with permission of The Royal Chemistry Society (2020).

pyrimidinone (UPy) [24,63,64] and N-(6-(3-(2,4-dioxo-3,4-dihydropyrimidin-1(2H)-yl)propanamido)pyridine-2-yl)undec-10-enamide (U-DPy) moieties [4,17,33]. The highly reversible nature of hydrogen bonding has enabled investigations into the folding processes that occur in SCNP formation. An SCNP system for pH responsive drug release was developed based on POEGMA-U-DPy [33]. The crosslinking of the SCNPs via the sextuple hydrogen bond array of the U-DPy dimers was shown to lead to stable particles. Drug release studies revealed that a combination of pH and temperature was needed for drug release. Polymer chain collapse via hydrophobic interactions have also been utilized to form SCNPs with a hydrophobic core and hydrophilic shell [17,65,66]. Pomposo and coworkers also exploit reversible metal complexation to achieve intramolecular chain interactions [26]. The acetoacetoxy ethyl methacrylate monomer contains β-ketoester which has shown the coordination with Cu(II) [26,34,67] as well as Fe(II) ions [13] which led to the formation of SCNPs.

3. Sequential folding

In the interest of controlled SCNP formation, sequential folding of polymer chains via utilization of two crosslinking strategies has been explored. Chao and coworkers used two different crosslinkers: first an amidation reaction was carried out, secondly a dithiol crosslinker was reacted in a thiol-Michael reaction [68]. The stepwise and sequential chain folding via light irradiation at different wavelength was investigated by Frisch et al., who selected two functional monomers that form homo-functional crosslinks at 415 and 470 nm (see Fig. 3) [25]. Sequential folding of *co*-polymers containing both BTA and UPy moieties was investigated, the BTA moieties in these *co*-polymers were located in the middle of the polymer chains and their self-assembly was controlled by a decrease in temperature [24]. On the other hand, UPy dimerization was initiated through light irradiation, which resulted in the protecting group being cleaved off, liberating the UPy moiety and allowing its assembly. The sequential folding of polymers offers control

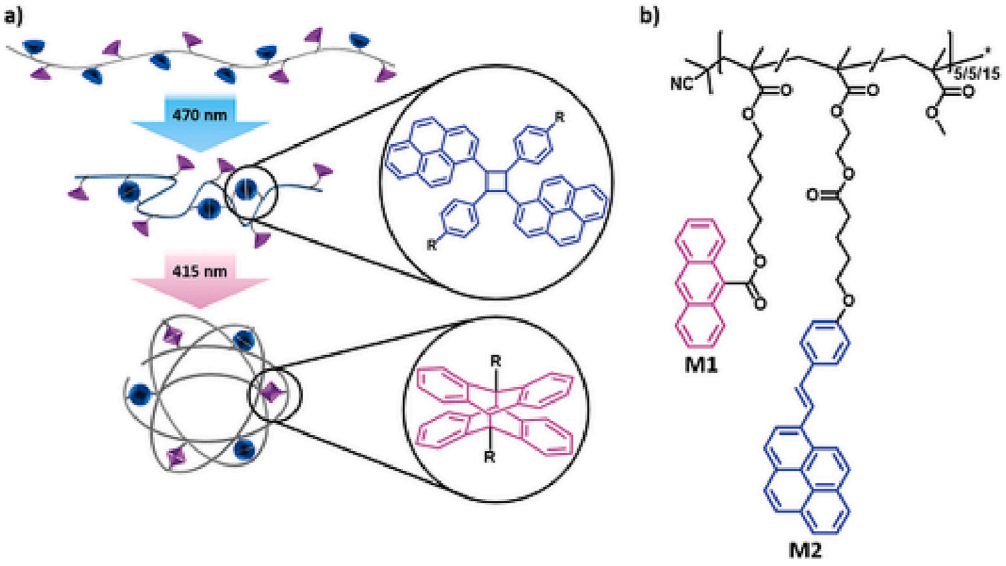

Fig. 3. a) Schema of sequential SCNP folding via selective wavelength induced crosslinking via homo-coupling of functional monomers; b) chemical structure of *co*-polymer. Reproduced with permission from ref. [25] with permission of John Wiley Sons, Inc. (2020).

over the density within the SCNPs [25]. Also, the formation of pockets has been explored utilizing sequential folding, which can be subsequently closed [24], this is of interest in the application of enzyme mimicry.

4. Upscaling SCNPs

In the effort to develop polymer nanoparticles for biomedical application, their production scale is typically a key challenge. The formation of SCNPs relies on intramolecular crosslinking, which is achieved in dilute polymer solution, but also requires large amounts of solvent [69]. Interestingly, exclusive intramolecular crosslinking of polymers has also been achieved under higher polymer concentrations (e.g. 2.5 mg/mL) as shown by Hawker and coworkers, who employed a continuous addition strategy that maintains a low concentration of crosslinkable polymer throughout the synthesis process, resulting in a high final SCNP concentration [11,30]. Based on this work, SCNP synthesis under milder conditions using thiol-Michael addition with a crosslinker solution and continuous polymer addition was developed by the Paulusse group, typically yielding 100–500 mg quantities [8]. The benign reaction conditions allowed SCNP synthesis both in organic and aqueous solvents [10,40]. Berda and coworkers applied the continuous addition strategy in the intramolecular crosslinking of polymers via atom transfer radical coupling of pendant alkyl or benzyl bromide functionalities resulting in gram-scale quantities of SCNPs [70]. Polymer concentrations of as low as 1–5 mg/mL and up to 100 mg/mL have also shown to produce SCNPs, for example by Terashima et al. [12] and Wong et al. [71], but the synthetic conditions are highly dependable on the chosen crosslinking route [69]. Barner-Kowollik and coworkers demonstrated upscaling of SCNP formation utilizing a flow system in which SCNPs are formed via a photo-activated crosslinking reaction [3]. This strategy uses a flow rate of 18.5 mL/min (yielding 540 mg/h) and a 5.5 min exposure time, this exposure time of UV radiation was shown to be significantly reduced as compared to the reported batch synthesis.

5. Functionalization of SCNPs

The use of polymers to form NPs has the great advantage of a virtually unlimited synthetic toolbox to introduce functionality on the NP surface [72]. SCNPs offer the ability to either incorporate the functional groups on the precursor polymers before SCNP formation, or afterwards in a post-formation functionalization (see Fig. 4).

5.1. Functionalization of polymer

A common functionalization route for SCNPs is utilizing activated ester containing polymers [73]. Pentafluorophenyl (PFP) moieties have shown highly controlled substitution reactions, which can be closely followed by ^{19}F NMR spectroscopy revealing release of pentafluorophenol [74]. Meijer, Palmans and coworkers prepared pentafluorophenyl acrylate homopolymers via RAFT polymerization [60]. These polymers are then functionalized with different functional amines to introduce an array of functionalities onto the polymer, including crosslinking abilities using BTA moieties [22], water-solubility by Jeffamine groups [22], dodecyl groups for hydrophobicity [58], as well as fluorescent dyes, such as Nile red [61] and Texas Red [22]. This strategy was also adopted by the Zimmerman and coworkers, who used PFP-polymers and functionalized them in a subsequent step with ammonium and carboxylic acid moieties, as well as azide groups to form covalently crosslinked SCNPs with a bifunctional diyne crosslinker [23,45,75]. Similar to the PFP-polymer strategy, poly(acrylic acid) (PAA) was synthesized as homopolymer for controlled functionalization [49]. Utilizing a Steglich esterification, PAA polymers were equipped with functional groups including tetrazole (Tet), maleimide (Mal) and triethylene glycerol monomethyl ether (TEG) containing hydroxyl groups. Functionalization via various strategies have been presented, it is important to note that the employed functionalization strategy needs to be chosen carefully to avoid hindrance of the SCNP formation.

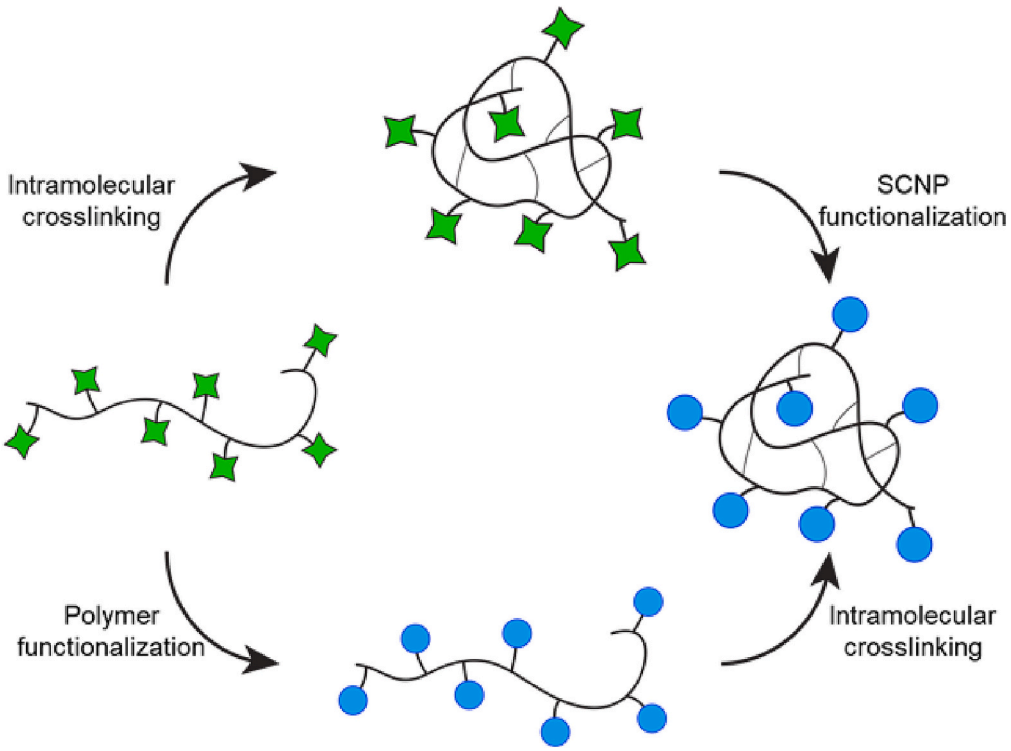

Fig. 4. Schematic presentation of SCNPs functionalization routes.

5.2. Post-formation functionalization of SCNPs

Post-formation functionalization of SCNPs with activated PFP esters has been utilized by Kröger et al., who *co*-polymerized pentafluorophenyl methacrylate with a protected thiol monomer for crosslinking, after which the thiols were deprotected and PFP-functional SCNPs were prepared via intramolecular thiol-Michael addition [40]. In a following step the SCNPs were conjugated with various functional amines including aminoglycerol, rhodamine ethylenediamine, L-alanine, L-gluthatione, and even combinations of functional amines were successfully conjugated at the desired ratio [40,76]. Loinaz and coworkers reported the conjugation of a peptide through its lysine group, which is used for targeting pancreatic cancer, to carboxylic acid groups on dextran SCNPs [37]. This amidation functionalization strategy was used to covalently bind a ligand for radiolabels to the dextran SCNPs to obtain radiolabeling with ^{67}Ga for SPECT imaging as will be discussed below [7]. Water solubility is an important first step towards biomedical application of SCNPs, but the required functionality is not always compatible with the employed crosslinking chemistry. Hydrolysis of various moieties has therefore been used to render SCNP systems water-soluble [9,10,77]. A variety of functionalization strategies has been developed that provide SCNPs with water-solubility or hydrophobicity, fluorescent labels, as well as targeting ligands, and high control over the functionality has been shown using PFP activated esters or click chemistry. The use of this chemistry to control cellular uptake and targeting will be further discussed in Sections 5.1 and 5.2.

6. SCNPs in biomedical applications

The biodistribution of SCNPs is an important factor that needs to be evaluated in view of future biomedical applications. While the investigation in biodistribution of SCNPs is still sparse, early indications regarding in vivo behavior of SCNPs has been reported. Song et al. studied the tumor targeting of single-chain tadpole polymers (SCTPs) and multi-tadpole assemblies (MTAs) in 4 T1 xenograft mouse models. [18] The results showed that the SCTPs did not show any accumulation at the tumor site, while the MTAs did show the highest tumor accumulation 12 h post intravenous injection. A strong signal of SCTPs was present in the liver 1 h post injection, while over a prolonged time the intensity in the whole body decreased. Analysis of major organs including kidney, lung, spleen, liver and heart by histological examination after the administration of PTX loaded MTAs, confirmed the absence of in vivo toxicity in mice. In comparison, SCNPs equipped with targeting peptides have been shown to accumulate at target tissue. Benito et al. prepared SCNPs with PTR86, a targeting peptide for somatostatin receptors which are overexpressed in pancreatic cancer, and studied targeting in tumor bearing mice after intravenous injection [37]. The SCNPs showed similar results in the first hours compared to the previous study, with high SCNP accumulation in the liver and lower accumulation in the bladder, 3 h after administration. While unlabeled SCNPs as well as PTR86 conjugated SCNPs were detected in the tumor after 3 and 24 h, only the SCNPs with the targeting peptide showed an increase in accumulation even 48 h post injection. Further in vivo toxicity studies showed a procoagulative effect at 100 mg/kg dose in mice, which resulted in thrombosis at the injection site. At 12.5 mg/kg the prevalence of thrombosis was reduced to one out of 5 mice and no systemic effects were present. The involvement of the liver in the clearance of negatively charged SCNPs from the blood circulation has recently been reported by Arias-Alpizar et al. on zebrafish embryos [78]. Earlier research revealed that various cell types of the liver, including liver sinusoidal endothelial cells (LSECs), are included in the clearance of small PEGylated quantum-dots [79]. Arias-Alpizar et al. reported that stabilin-1 receptors, which are located on scavenging endothelial cells (SECs), a cell type homologous to LSECs, are involved in the clearance of SCNPs in zebrafish embryos [78]. The size of NPs has shown to have an influence on the clearance, as larger NPs of around 100 nm were predominantly cleared by Stabilin-2 receptors. Further research into the biodistribution and clearance of SCNPs is required to better predict their potential in biomedical applications. On the cellular level, controlling cellular uptake of SCNPs is key in biomedical applications to achieve the imposed purpose of the nanocarriers. Particle size is key for cellular uptake, as the high surface to volume ratio and increased curvature of SCNPs provide a greater contact area with cell membranes compared to larger NPs, which results in increased uptake [80,81]. Chen et al. compared cell uptake of SCNPs to unfolded polymer chains in human mesenchymal stem cells (hMSCs), and showed increased cellular uptake for SCNPs as compared to unfolded polymers [82]. Furthermore, studies into the physical characteristics of SCNPs have revealed a state between flexible and rigid nanoparticles; both states are present within various locations in a single SCNP [15,83]. These characteristics are shared with intrinsically disordered proteins (IDP) [84,85]. Although in IDPs the ordered regions that are stabilized by physical interactions may break under shear flow, while the equivalent crosslinked domains in SCNPs show higher integrity under shear flow [31]. One of the major concerns for supramolecularly crosslinked SCNPs for biomedical applications is their stability in complex media. Deng et al. investigated the stability of Nile red conjugated SCNPs crosslinked through hydrogen bonding BTA moieties or solely based on hydrophobic interactions of Jeffamine@M-1000 in PBS, DMEM and DMEM supplemented with 10% FBS [61]. Based on CD spectra, DLS and absorbance measurements the supramolecular crosslinks are stable in all three media, only in DMEM supplemented with 10% FBS leakage of encapsulated Nile red was observed, while the particles remained stable. Particle stability was further analyzed in HeLa cells, where the particles were delivered into the lysosomes or the cytoplasm via electroporation. While spectral confocal microscopy showed that SCNPs retained their folded structures in the cytosol, the SCNPs formed solely via hydrophobic interactions disintegrated in lysosomes and only SCNPs containing crosslinks based on hydrogen bonding of BTA moieties remained their folded conformation. These results address the concerns on the stability of supramolecular crosslinked SCNPs and emphasize the importance of studying the stability of other crosslinking motifs.

6.1. Cell targeting

Targeting of specific cells is a crucial challenge in biomedical applications in order to achieve high local concentrations of therapeutics. Targeting ligands are typically employed to direct uptake by specific cells. Cancer cells, such as HeLa cells, have a high expression of GLUT receptors [86]. Kröger et al. chemoenzymatically synthesized three glucose monomers to study the uptake behavior of a series of analogous glucose-SCNPs [87]. The glucose-moieties were conjugated either on position C1 or C6; C1-conjugation blocks the opening of the glucose to obtain the linear form, which was, however, shown not to inhibit GLUT receptor mediated uptake [88]. The glucose monomers were *co*-polymerized with a xanthogenate methacrylate for covalent SCNP crosslinking. Cellular uptake was observed for all three resulting SCNPs, although the blocking of the C1-position of glucose decreased internalization in HeLa cells. CLSM confirmed an increase in uptake of glucose SCNPs functionalized via position C6, and strong co-localization with late endosomes and lysosomes was observed after 4 h incubation. However, investigations into the uptake mechanism are required to identify interactions of the glucose moieties with GLUT receptors. Different sugar molecules are also interesting for biological applications, and the synthesis of mannose-functional [47,59,89] and galactose-functional [59,89] SCNPs has been shown. The mannose SCNPs were further used to functionalize nanodiamonds, CLSM images of RAW 264.7 macrophages presented the internalization of the nanodiamonds decorated with SCNPs [47]. Specific receptor targeting was also utilized by Baij et al. for cell labeling and imaging of human breast cancer (SK-BR-3) cells, which display high expression of human epidermal growth factor receptor (HER2) (see Fig. 5) [90]. SCNPs were functionalized with

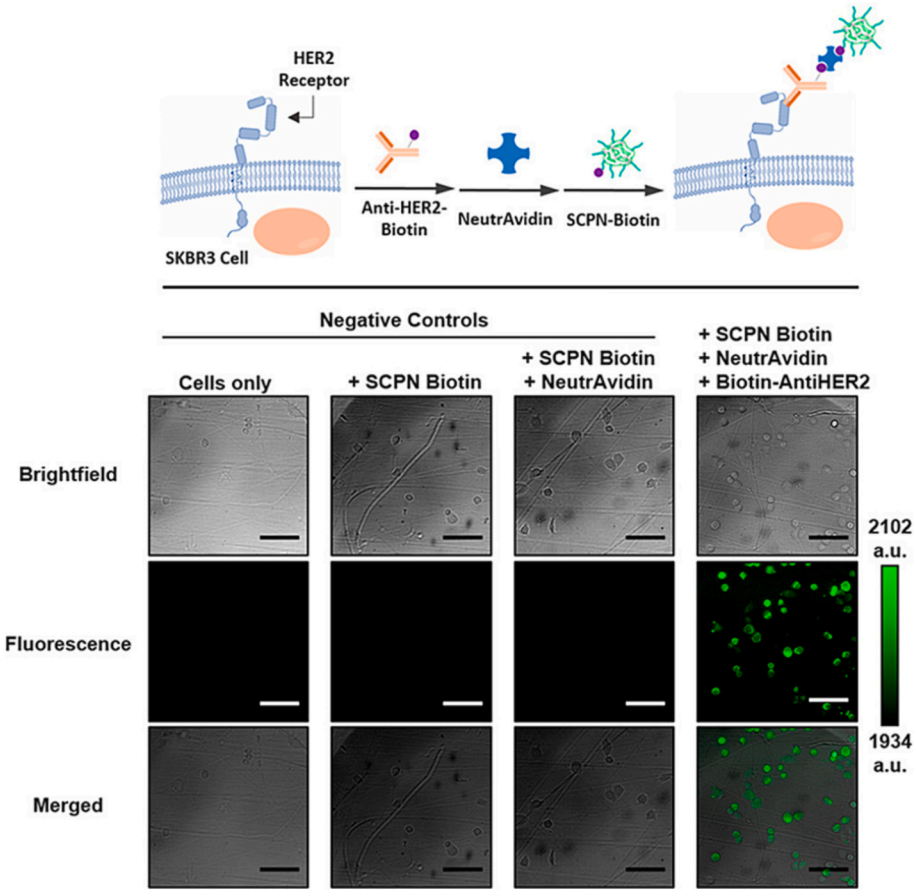

Fig. 5. Scheme of targeted cell labeling and microscopy results of fluorescent labeling of SK-BR-3 breast cancer cells utilizing SCNPs and microscopy images of cell labeling, scale bar 100 μm. Reproduced with permission from ref. [90] with permission of American Chemical Society (2019).

biotin to bind an Anti-HER2-Biotin antibody via sandwich binding with NeutrAvidin and successful cell labeling was demonstrated for the SCNPs. Specific cellular uptake was further studied using SCNPs based on a poly(epichlorohydrin) (PECH) backbone with PEG pendant groups in HeLa and NIH/3 T3 cells, and enhanced cellular uptake of the PEG-PECH SCNPs was observed in this cancer cell line [17]. Cellular uptake in HeLa cells was further increased by using SCNPs conjugated with folic acid. The presented research establishes the advantages of targeted cellular uptake utilizing surface modifications on SCNPs. Further research in the optimization of surface functionalization for targeted cell interactions is needed to reach optimal interactions of SCNPs with specific cells, as multivalent interactions of ligands and targets have been shown to increase cellular uptake [91]. In order to direct SCNP research to high potential targeted nanocarriers, biodistribution studies are required to better understand their behavior in vivo.

6.2. Cellular uptake

Size dependent cellular uptake of SCNPs has been systematically studied by Bai et al. [77] Using glycerol functionalized SCNPs with sizes ranging from 7 to 40 nm, increases in particle uptake for smaller SCNPs was demonstrated in Hela cells by flow cytometry after 3 h incubation, with the highest uptake observed for the smallest, 7 nm SCNPs, highlighting the advantage of SCNPs in cellular uptake. However, as flow cytometry does not differentiate between SCNPs binding to cell surfaces and SCNPs that are actually internalized, further investigations are required to confirm the presented trend. The group of Zimmerman developed SCNPs with catalytic activity, for both intra- and extracellular applications, by carefully altering the functional groups on the SCNPs [23,31,45]. To achieve intracellular delivery, SCNPs were functionalized with 60 to 70% of quaternary amines providing a permanent positive surface charge, which promotes the internalization of SCNPs via interactions with the negatively charged cell membrane [23,45]. This resulted in endosomal uptake and the SCNPs were shown to be prone to remain in endosomal structures in the cells. The SCNP system for extracellular catalytically activity, which will be discussed in Section 6.8, was functionalized with 70% of PEG units [45]. PEGylation is a common surface functionalization of NPs for biomedical applications, leading to prolonged blood circulation times by avoiding cellular uptake [92]. This was also shown for these SCNPs, as the PEGylating of SCNPs significantly decreased uptake by HeLa cells [45]. Palmans and co-workers investigated the delivery of supramolecularly crosslinked SCNPs to different compartments in HeLa cells [22]. The SCNPs were conjugated with 83% Jeffamine functional groups on the surface to provide water solubility. However, this molecule also causes a reduction in cellular uptake as previously presented for PEGylated SCNPs [45]. After 3 h incubation no SCNPs were present in HeLa cells as shown in Fig. 6a [22]. In order to reach specific subcellular locations with the Jeffamine-coated SCNPs, the experimental conditions were varied. Endosomal uptake of SCNPs was achieved at increased particle concentration and after prolonged incubation times, i.e. using 2.0 mg/mL to 2.5 mg/mL concentrations and a 24 h incubation period (Fig. 6b) [22,61]. CLSM images revealed that the SCNPs were co-localized with lysosomes. Cytosolic delivery of the Jeffamine functionalized SCNPs was achieved by means of electroporation, resulting in strong SCNP signal throughout the HeLa cells (Fig. 6c) [22]. However, cell death resulting from mechanical stress of the cells due to the application of electrodes was also observed.

The surface chemistry on SCNPs determines the mode of interaction with cell membranes, for example, glycerol-functional SCNPs were

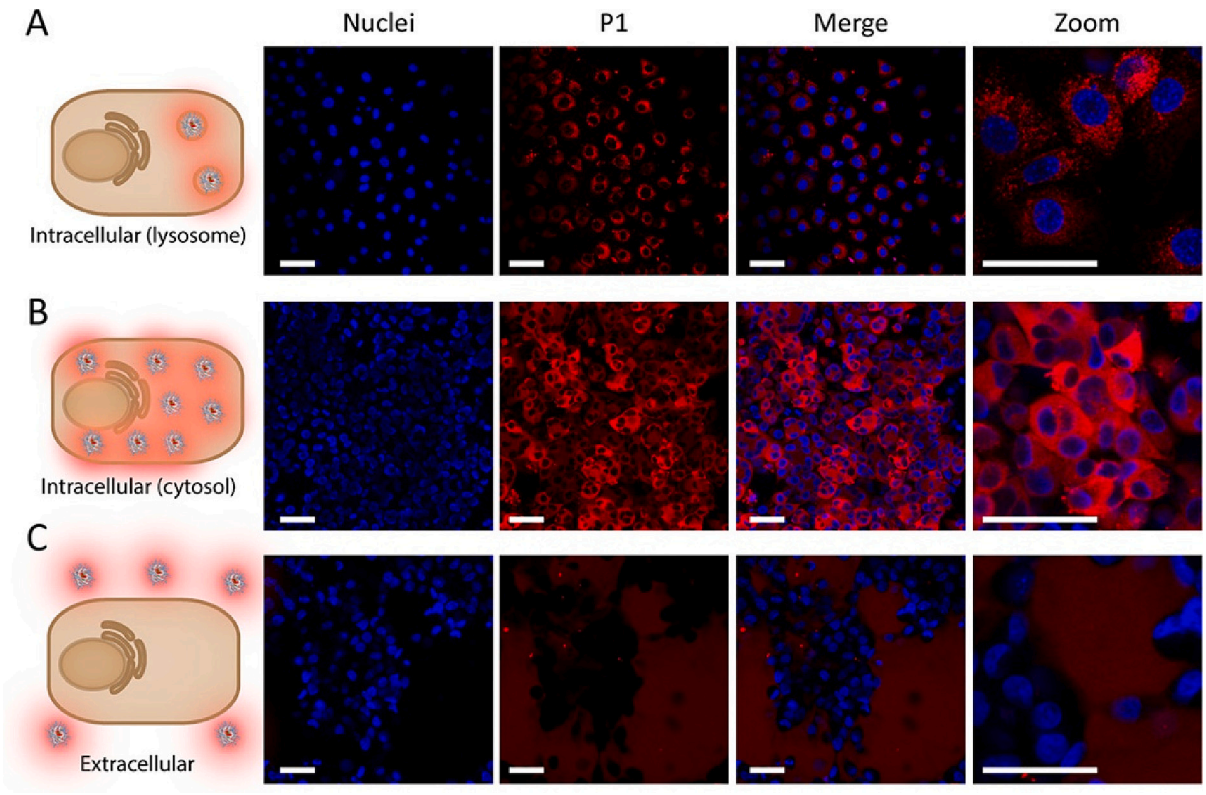

Fig. 6. Confocal images of HeLa cells incubated with SCNPs a) at high concentration 2.5 mg/mL for 24 h, b) under electroporation or c) at 1 mg/mL for 3 h. Nuclei were stained in blue and SCNPs were labeled with Texas Red, scale bar 50 μm. Reproduced with permission from ref. [22] with permission of American Chemical Society (2018). (For interpretation of the references to colour in this figure legend, the reader is referred to the web version of this article.)

shown to be internalized via endosomal route, while displaying high biocompatibility [10]. However co-localization of SCNPs with lysosomes was observed as well. Positive surface charges, for example quaternary amines, have been shown by Chen et al. to enhance cellular uptake of SCNPs [45]. SCNPs with positive surface charges, induced by a molecular dendritic transporter containing guanidine moieties, achieved efficient cellular uptake after 30 min incubation with 4 μM of SCNPs [35]. CLSM images confirmed that the dendritic transporter was crucial for cellular uptake of SCNPs in mouse fibroblast (NIH/3 T3) cells. Further, the CLSM images revealed cytosolic delivery of SCNPs, as the guanidine moieties combine the ability of protonatable amines that induce endosomal escape, known as proton sponge effect, while maintaining high cell viability. The cytosolic delivery of SCNPs was further explored by Hamelmann et al. with a particle set containing increasing amounts of tertiary amines introduced by *N,N*-dimethylethylene diamine (DMEN) (0, 15, 30, 45 and 60%) in mouse brain endothelial (bEND.3) cells [76]. Flow cytometry showed a strong increase in uptake for SCNPs functionalized with 45 and 60% tertiary amines already after a 1 h incubation. Furthermore, CLSM revealed that the SCNPs with 45 and 60% of DMEN were released in the cytosol as shown in Fig. 7, whereas SCNPs with 0 to 30% of tertiary amines remained present in intracellular clusters which co-localized with lysosomes. These results demonstrate that careful alteration of the surface functionality on SCNPs can even provide control over their subcellular location.

The presented research emphasizes the importance of protonatable functional groups on the SCNPs for their cytosolic release. For quaternary amines, even though the positive charge induced cellular uptake, the SCNPs were not released into the cytosol [45]. Protonation of amines

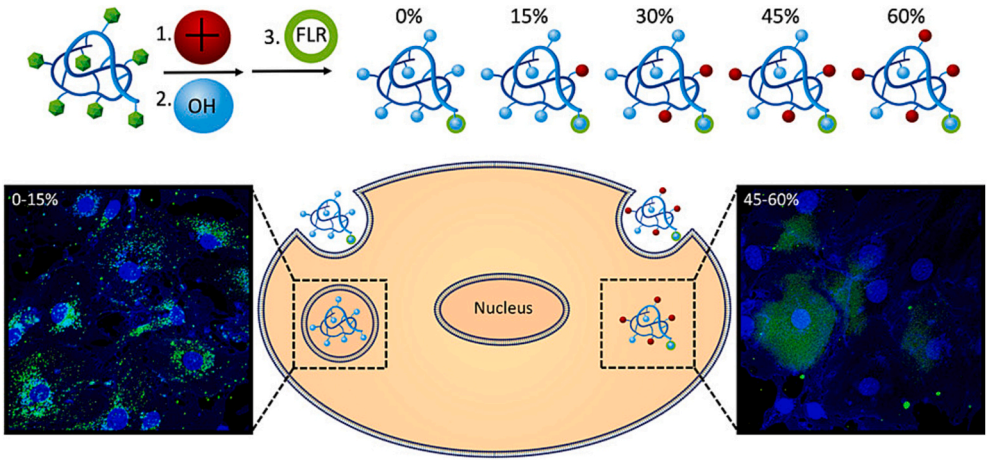

Fig. 7. Schematic presentation of SCNP functionalization and the final particle set with different amounts of tertiary amines, described by percentages; illustration of subcellular location of SCNPs after incubation 6 h at 50 μg/mL for left panel and 1 h at 50 μg/mL for right panel with HeLa cells, nuclei and cell membrane were stained in blue. Reproduced with permission from ref. [76] with permission of American Chemical Society (2021). (For interpretation of the references to colour in this figure legend, the reader is referred to the web version of this article.)

on the SCNPs presumable induces a proton sponge effect [93] and leads to endosomal escape of SCNPs [35,76]. Combination of cell targeting and directing the intracellular location of SCNPs may enhance the local concentration of SCNPs at selected tissues to more effectively combat diseases and further avoid degradation of the therapeutics in lysosomes. In the future, investigation into uptake mechanism of SCNPs including the receptor SCNP interactions and internalization will extend the knowledge on SCNP behavior on a cellular level.

6.3. Drug encapsulation and release

The encapsulation abilities of SCNPs have been investigated for various systems, including covalently and supramolecularly crosslinked SCNPs. One of the most common model drugs used to study the encapsulation behavior of SCNPs is Nile red [10,53,58,61,94], which is poorly water soluble, but when encapsulated in SCNPs the dye can indicate the hydrophobicity of the interior in aqueous solutions. Many drug candidates fail due to their poor water solubility, therefore Kröger et al. developed a SCNP system that is able to encapsulate dug molecules irrespective of their polarity [10]. In this study Nile red was encapsulated in covalently crosslinked SCNPs in either organic and aqueous solutions. Kröger et al. presented SCNPs based on a *co*-polymer containing solketal units, which allow for carrying out the intramolecular crosslinking reaction either in organic solvent and subsequently render the particles water-soluble by hydrolyzing the solketal groups, or in aqueous solution by first hydrolyzing the co-polymer and crosslinking it afterwards [10]. In this work, the encapsulation of Nile red via both pathways was confirmed via a GPC coupled fluorescence detector. Furthermore, rifampicin, a broad-spectrum antibiotic with poor water-solubility, was encapsulated at a drug loading of 16 wt%, analyzed by UV–Vis, which corresponded with 81% entrapment efficiency. The Pomposo group showed the encapsulation of a variety of drug molecules, including cisplatin [95], lovastatin [95], folic acid [96], hinokitiol [96] and vitamin B9 [19] in different SCNP systems. Cisplatin loaded povidone SCNPs showed no significant difference in size and zeta-potential compared to neat povidone SCNPs [95]. The drug release was analyzed by UV–Vis, and showed 28% release within 2 h and up to 95% release after 48 h in water. In the case of Vitamin B9 loaded "Michael" SCNPs a drug loading of 41 wt% was achieved and complete drug release within 5–6 h in water with neutral pH was observed [19]. SCNPs based on PEOGMA-U-UPy polymers crosslinked through hydrogen bonding were used to encapsulate 5-fluorouracil (FU) at a drug loading of 20 wt% [33]. These SCNPs showed a size increase from 23 nm to 91 nm upon encapsulation as determined by DLS. This size increase is likely due to the reversible nature of the hydrogen bonds, which can lead to the interaction of multiple SCNPs and therefore the formation of aggregates. The drug release was studied in vitro based on temperature and pH. At 37 °C and pH 7 a slow release of 19% in PBS after 30 h. An increase in temperature to 42 °C caused only a slight increase in the drug release to 24%. Also, the drug release remained low at 26%, when the pH was lowered to pH 4, while the temperature was kept at 37 °C. Only, with a combination of temperature and pH change to 42 °C and pH 4 a more rapid drug release was observed obtaining 53% release after 10 h and 69% after 30 h. Indicating that the sextuple hydrogen-bonded U-DPy dimers are responsive to temperature increase and lowered pH, but only the combination of both causes the dimers to dissociate efficiently. Cheng and co-workers evaluated PEG-PECH self-assembled SCNPs in the encapsulation of doxorubicine (DOX) for application in cancer therapy [17]. A size increase was observed upon functionalization of PECH with folic acid, from a particle diameter of 11.2 nm to 28.6 nm as measured by DLS. The zeta-potential also increased significantly from 2.6 mV to 25 mV. Drug loading with doxorubicin further changed the particle characteristics, as the sizes of bare and folate-conjugated SCNPs roughly doubled to respectively 25.3 nm and 52.9 nm. Drug loadings of around 15 wt% were achieved. These results indicate that drug encapsulation can lead to a particle size increase, this behavior however is strongly dependent on the particle system and the employed crosslinking strategy. The dynamic supramolecular crosslinking may lead to formation of non-unimolecular structures upon encapsulation. Efficient drug encapsulation has been shown for various SCNP systems. However, in some cases an increase in size upon drug encapsulation has been observed. As the size is a key characteristic of SCNPs, changes in particle size could lead to different behavior regarding cell interactions and biodistribution behavior.

Although drug encapsulation is a versatile strategy, it is not always effective for every drug molecule and the use of drug-conjugates or prodrugs can offer advantages regarding drug loading, control over release and efficacy. An example of drug conjugation onto SCNPs was developed by Gracia et al., who prepared a Tn-Antigen mimetic 5, which is studied as anticancer vaccine, and conjugated it onto dextran (DXT) SCNPs as a potential anticancer vaccine [41]. The Tn-Antigen mimetic 5 was first conjugated to a fluorinated PEG linker with a protected amine group, which was subsequently used to couple the compound to DXT SCNPs. The conjugation was followed by ^{19}F NMR. Addition of the Tn-Antigen caused an increase in particle diameter from 16 nm for the dextran SCNPs to 70 nm for the functionalized SCNPs as measured by DLS. The in vitro evaluation of the Tn-DXT SCNPs presented a triggered release of IL-6 from human peripheral blood mononuclear cells (PBMC). This study further revealed a similar innate immune response triggered by the Tn-DXT SCNPs compared to naturally present Tn clusters. Drug loading via conjugation onto SCNPs has also been shown via NHS ester chemistry for doxorubicin [97] and via prodrug formation for atovaquone [98]. In the future, control over drug release rate and stimuli responsive release can be introduced by utilizing linker molecules. This strategy was shown by the group of Stayton introducing various linker on prodrugs forming polymers that have shown to modulate the release rate and tuning the release to be stimuli responsive [99–101].

6.4. SCNPs in drug delivery

Research on SCNPs in controlled drug delivery has shown a variety of approaches towards drug encapsulation and release. However, studies into the evaluation of SCNPs as drug carriers in specific diseases is still limited.

SCNPs delivering therapeutics for cancer therapy have been evaluated by Chen et al. who developed DOX-loaded PECH-PEG SCNPs [17]. The DOX-loaded SCNPs were evaluated on HeLa cancer cells, as well on the non-cancer cell line NIH/3 T3. Higher uptake of the DOX-loaded SCNPs was observed in HeLa cells as compared to NIH/3 T3 cells. The DOX-loaded PECH-PEG SCNPs did not significantly decrease cell viability in NIH/3 T3 cells, as cell viability remained above 70% even as the concentration increased to 40 μg/mL (see Fig. 8a). Contrary, DOX-loaded PECH-PEG SCNPs showed an inhibitory concentration (IC_{50}) of 8.27 μg/mL in HeLa cells after 24 h incubation (Fig. 8b). For free DOX the IC_{50} in HeLa cells was 1.86 μg/mL. These results indicate that the DOX-loaded PECH-PEG SCNPs present high toxicity to cancer cells, while expressing low toxicity to fibroblasts. Conjugation of the SCNPs with folic acid resulted only in a minor decrease in IC_{50} (7.96 μg/mL).

Further exploration of SCNPs in cancer therapy has been conducted by Song et al. using single-chain tadpole polymers (SCTP), a variant of SCNPs containing a non-crosslinked polymer 'tail', which are in the same size range with a particle size of 10.8 nm (see Fig. 9a) [18]. These paclitaxel (PTX) loaded SCTPs formed reversible multi-tadpole assemblies (MTAs) of 76.9 nm. The PTX drug loading was 5.6 wt%, with an encapsulation efficiency (EE) of 71.2%. The tumor penetration of MTAs at pH 6.9 and 7.4 was investigated in U87MG multicellular tumor spheroids (MCTS). The results showed homogenous fluorescence throughout the tumor at pH 6.9, while at pH 7.4 the fluorescent signal was mostly present on the exterior margins of the tumors, indicating that disassembly of MTAs leads to improved tumor penetration (see Fig. 9b). Incubation of breast cancer (4 T1) cells with MTAs also resulted in higher internalization at pH 6.9 than at pH 7.4 after 4 h incubation.

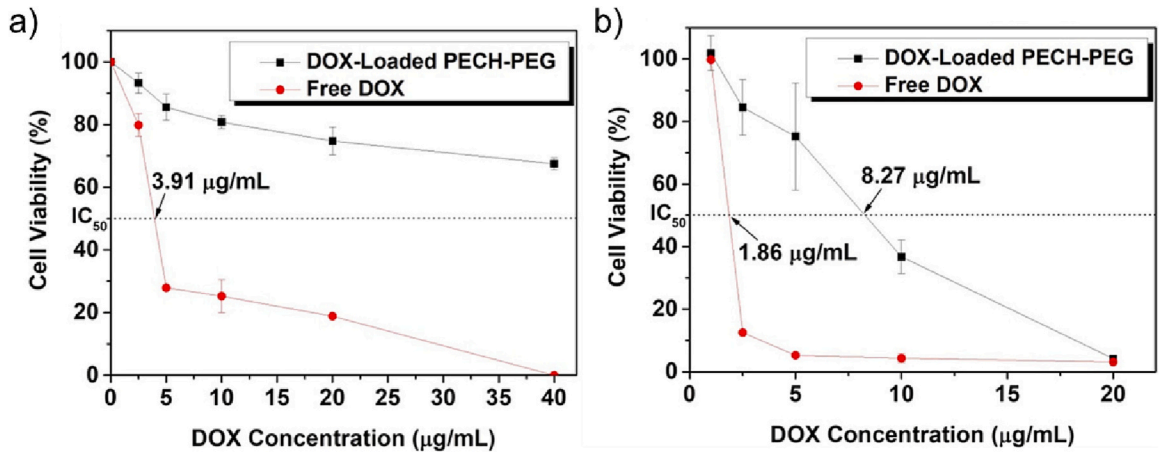

Fig. 8. Cell viability of (a) NIH/3 T3 and (b) Hela cells incubated with DOX-loaded PECH-PEG SCNPs and free DOX. Adapted from ref. [17] with permission of American Chemical Society (2021).

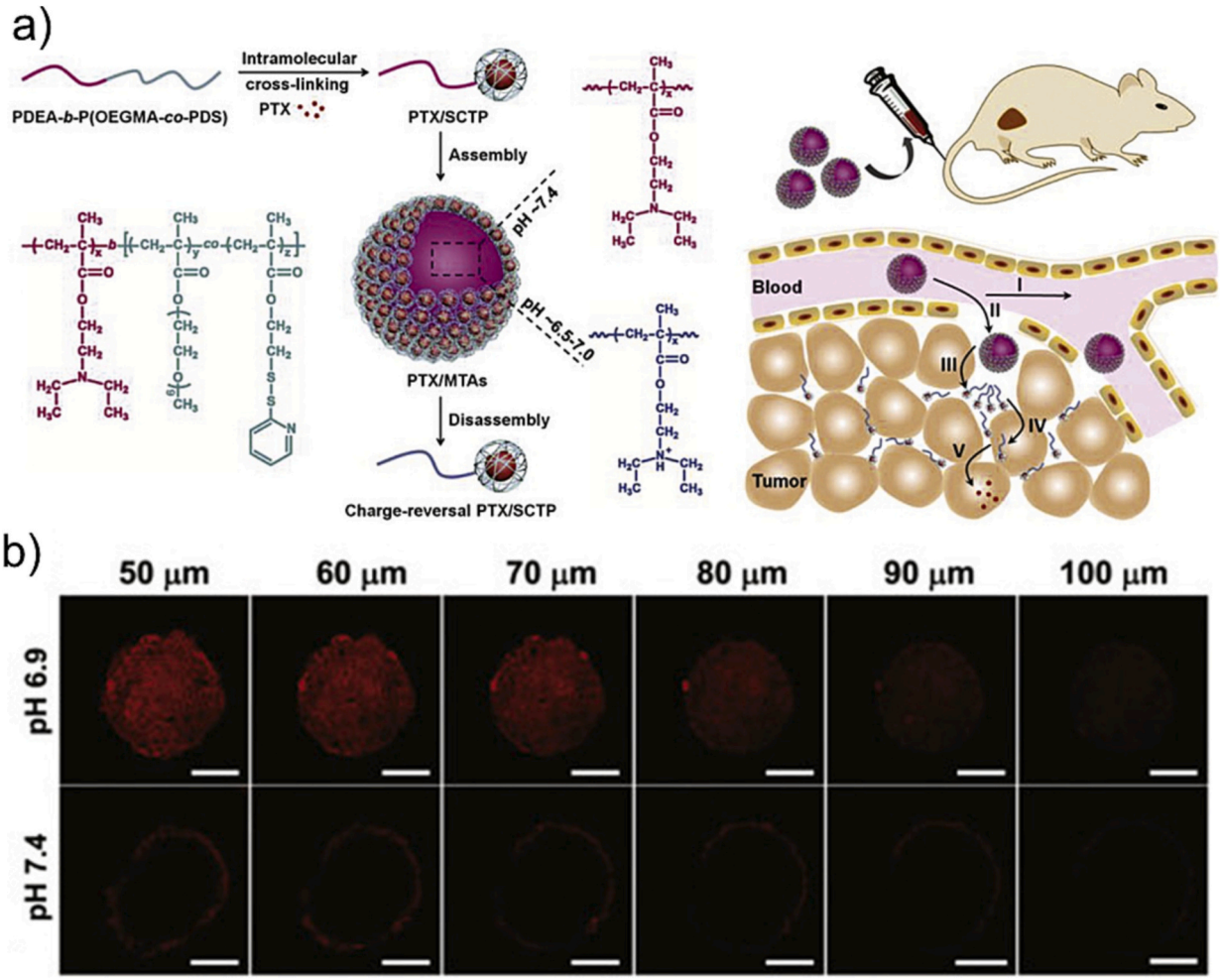

Fig. 9. a) Illustration of the preparation of tadepole SCNPs and the self-assembly of MTAs and schematic presentation of MTAs with degradation into SCNPs upon entry in tumor tissue; b) Confocal images of MCTS for the ex vivo penetrating evaluation, MTAs for 4 h at pH 6.9 (top panel) and pH 7.4 (bottom panel) were incubated with MCTS and *Z*-stacks were recorded, scale bar 200 μm. Adapted from ref. [18] with permission of Elsevier.

Tumor targeting of MTAs and SCTPs was analyzed in BALB/c nude mice bearing 4 T1 xenografts after intravenous injections. Initially, a strong signal for both NPs was observed in the liver 1 h post injection. The signal of SCTPs decreased with prolonged time and did not occur at the tumor site. In contrast, the highest accumulation of MTAs at the tumor site was observed 12 h post injection. Efficacy studies of PTX-loaded MTAs in BALB/c nude mice bearing 4 T1 xenografts showed tumor growth in mice injected with PBS and only minor tumor growth inhibition for mice injected with free PTX, whereas injection with PTX loaded MTAs resulted in 82% tumor suppression. The current limited

results of SCNPs in controlled drug delivery have shown the potential of SCNPs in this field. The growing research in the fields of drug loading by encapsulation and conjugation as well as cell targeting and cellular uptake may lead to an expansion of the applications of SCNPs in controlled drug delivery in the future.

6.5. Antibacterial SCNPs

Antibiotic resistance is a growing concern to our society and antimicrobial nanoparticles have accordingly attracted considerable attention. Polymer nanoparticles mimicking antimicrobial peptides (AMPs) have been developed, by integrating both cationic and hydrophobic side chains [102]. These functionalities in AMPs are known to cause membrane disruptions, and this has also been shown for the NPs. Nguyen et al., explored the antimicrobial activity of SCNPs consisting of oligoethylene glycol (OEG), and different amine and hydrophobic groups with consistent ratios [20]. The SCNPs were formed by self-folding hydrophobic interactions in water. SCNP activity against the Gram-negative bacteria *Pseudomonas aeruginosa (P. aeruginosa)* and *Escherichia coli (E. coli)* was evaluated in relation to the functional groups on the SCNPs. SCNPs with increasing hydrophobicity showed higher antimicrobial activity against the pathogens by cell membrane disruption, which is in line with research on polymer NPs presenting higher antimicrobial activity with increasing hydrophobic content [20,103]. Two different linker lengths for the amine functionality were studied, and the shorter linker presented higher antimicrobial activity. The SCNPs presented a fast rate of eradicating planktonic microbial cells with over 99% efficiency in 1 h, as well as dispersion of the biofilm, which was shown at a rate of ca. 72% after 1 h. Tian et al. recently evaluated SCNPs with high local charge densities as a coating with improved bactericidal activity and antifouling characteristics [21]. The SCNPs were synthesized from a precursor block *co*-polymer of PEG and cationic polypeptide elements, using 1,4-diiodobutane as a crosslinker that quaternizes the amines. To form a surface coating, a polydimethylsiloxane (PDMS) surface was first coated with polydopamine (PDA) and subsequently dipped in the aqueous SCNP solution to form a SCNP surface layer. The interaction of PDA and SCNPs was described as a composition of interaction including hydrogen bonds, cationic/π-π interactions and covalent bonds formed via Michael addition. Bactericidal activity of the SCNPs was first evaluated in solution. Both the precursor polymer, as well as the SCNPs were shown to inhibit the growth of *Staphylococcus aureus* (*S. aureus)* (Gram-positive) and *E. coli* (Gram-negative) at low concentrations of 50 μg/mL. The SCNPs presented slightly higher antibacterial activity than the polymer, as shown by optical density measurements after 24 h incubation. This was attributed to the smaller aggregation size and the higher local charge density after the SCNP formation. Excellent antibacterial activity of the SCNPs on the coated surfaces was demonstrated in a contact assay, as no surviving bacteria were observed for either strain. However, also the precursor polymer killed 99.9% of *S. aureus* and *E. coli*. SCNPs have been used as nanoreactors in antibacterial applications and Zimmerman and coworkers utilized Cu(II)-SCNPs, that catalyze the azide-alkyne click reaction, in bacterial growth inhibition, by conjugating two substrates to form the antimicrobial bisamidine (see Fig. 10a) [104]. This resulted in strong growth inhibition of *E. coli* when incubated with the substrates, nanoreactor and sodium ascorbate (see Fig. 10b).

Falciani et al. presented dextran-based SCNPs encapsulating SET-M33 peptide, a non-natural antimicrobial peptide, for *P. aeruginosa* inhalation therapy [105]. A biodistribution study in rats revealed a prolonged residence time for the peptide loaded SCNPs as compared to the free peptide. Complete eradication of *P. aeruginosa* in a pneumonia mice model was achieved only at a high concentration of 5 mg/mL, which is similar to the free peptide.

The antimicrobial activity of SCNPs based on their surface functional groups and the ability of SCNPs to act as nanoreactors have shown promising results. Further research is needed to investigate the biocompatibility of SCNPs with high positive charge densities. An interesting advantage of SCNPs in antibacterial applications is their size, which is in the range of that of AMPs. A combined approach, in which antimicrobial activity in the SCNP structure is combined with an antibiotic cargo, may prove effective. Additionally, equipping the SCNPs with targeting ligands may lead to an increase in local SCNP concertation, which leads to further advancing the antibacterial efficiency of SCNPs. [106]

6.6. SCNPs in targeted imaging

The use of SCNPs in targeted imaging requires incorporation of a contrast agent or imaging agent, but also a favorable biodistribution behavior, and ideally even targeting specific tissues. Molecular imaging is commonly used in the clinic in disease diagnosis, following disease progression and assessing the effectiveness of medical interventions. Benito et al. integrated the gamma emitter ^{67}Ga by chelation in SCNPs based on poly(methacrylic acid) equipped with the somatostatin analogue PTR86 as targeting ligand for pancreatic tumors [37]. The potential of the radiolabeled SCNPs as imaging agent was evaluated in a

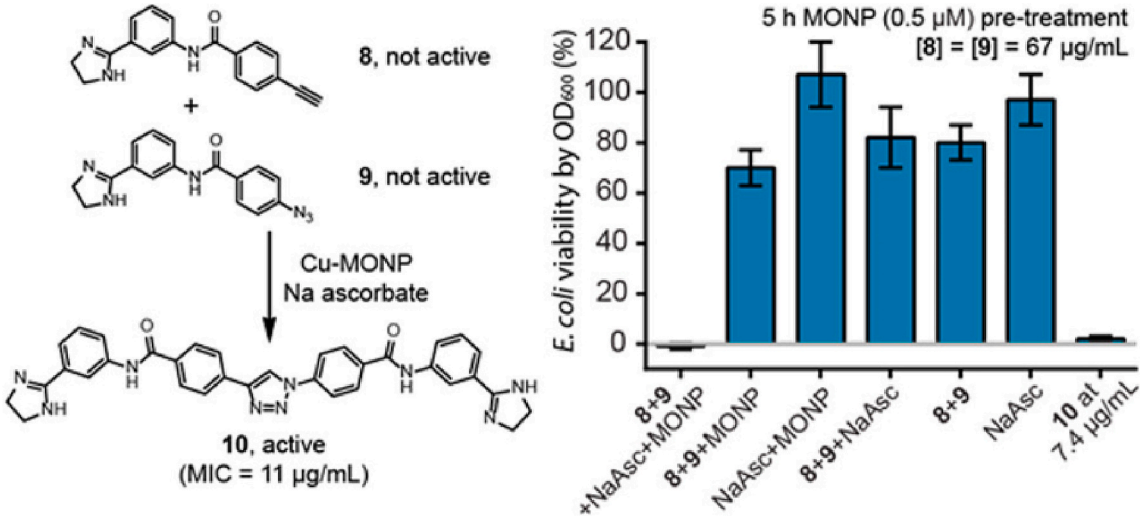

Fig. 10. Nanoreactor induced intracellular synthesis of antimicrobial bisamidine 10 from substrates 8 and 9 in *E. coli* catalyzed by NaAsc = sodium L-ascorbate. Adapted from ref. [99] with permission of American Chemical Society (2016).

xenograft mouse model of human pancreatic adenocarcinoma. SPECT imaging with co-registration CT imaging revealed good retention of the PTR86 conjugated SCNPs at the tumor site as shown in Fig. 11. Radiolabeled dextran-based SCNPs were successfully employed in the evaluation of the regional lung distribution of an aerosolizer in vivo in a rodent model [7]. The results further indicated that the administration protocol was successful, although some regions in the lung remained underexposed. Therefore, further optimization of the distribution of SCNPs by the aerosolizer is required. Radiolabeling of SCNPs has been shown to be an effective imaging strategy for in vivo applications [37,107]. Imaging agents with paramagnetic properties are suitable for MRI imaging and the use of SCNPs for imaging has been investigated. Specifically, SCNPs loaded with Gd(III) ions have been explored as contrast agents [9,108]. Perez-Baena et al. presented the controlled integration of multiple Gd(III) ions in SCNP, by integrating the Gd(III) ions in the crosslinker [9]. The SCNPs were based on an acrylic *co*-polymer and particle formation was achieved with a bifunctional diethylenetriaminepentaacetic acid (DTPA) containing crosslinker. The DTPA groups were later loaded with Gd(III) ions to obtain paramagnetic SCNPs for MRI. This method enabled successful integration of multiple Gd(III) ions in sub 5 nm NPs, wherein the amount of Gd(III) ions could be adapted by varying the molecular weight of the precursor polymer. The relaxivity value r_1 for the Gd(III)-SCNP per Gd molecule was 4-fold higher compared to the Gd-loaded crosslinker.

Cell labeling has been achieved with many fluorophores, in the work of Liu et al. an amphiphilic polymer was used to form SCNPs in aqueous solution, forming a hydrophobic interior which contains a single fluorophore [109]. The incorporation of fluorophores that emit in the red and near-infrared regions was shown to achieve fluorescence quantum yields in aqueous solution similar to benchmark fluorophores in toluene. In further research, a fluorescence quantum yield of at least 70% for hydrophobic fluorophores in PBS was obtained, using a single moiety of perylene-monoimide in SCNPs [110]. The work of Li et al. was directed towards developing brighter fluorophores with greater stability in SCNPs [111]. By introducing dendron structures of polyglycerol on the polymer the water-solubility of the SCNPs increased, which increased the photo-stability of the fluorophores. In recent work, SCNPs containing a fluorescent core were shown to display aggregation-induced emission (AIE) [112]. These materials avoid quenching due to aggregation and possess high photostability.

Successful incorporation of a variety of imaging modalities, such as radiolabels, paramagnetic compounds and fluorophores, into SCNPs has been demonstrated, enabling localization of SCNPs in vitro and in vivo. Initial in vivo studies have shown promising results regarding the use of SCNPs as imaging agents. However, detailed investigations into the biodistribution behavior of SCNPs are still scarce and further investigations are essential for future application.

6.7. SCNP folding resembling proteins

The function of proteins is directly linked to their 3D structure, which is obtained through four distinct stages of folding of a polypeptide chain. Hydrogen interactions lead to the formation of α-helices and β-sheets, which build towards 3D structures containing hydrophobic and hydrophilic regions. The polymer chain folding observed for SCNPs resembles protein folding [113]. Supramolecular SCNP systems additionally enable investigation of the dynamic properties of protein folding. Terashima et al. used a *co*-polymers of PEG and BTA pendant groups to form supramolecularly folded SCNPs through the intramolecular interactions of BTA units [12]. The BTA units have been shown to fold into helical structures, resembling those observed in proteins. As discussed above, various researchers have developed SCNPs with sequential polymer folding to increase their resemblance with protein structures [114]. In the example of Hosono et al., the self-assembly of BTA units in the middle of the ABA block *co*-polymer was controlled by a temperature change and subsequently the ends of the polymer chains were linked by UPy dimer formation forming SCNPs (see Fig. 12) [24]. Both of these crosslinking methods are based on supramolecular interactions and this work is an excellent example of the research that has been done regarding controlled folding of SCNPs to mimic the combination of supramolecular interactions in the peptide chains of proteins, such as Van der Waals interactions, hydrophobic interactions, hydrogen bonding and ionic bonding. The group of Pomposo were the first to focus on SCNPs mimicking intrinsically disordered proteins (IDPs) and compared chain collapse of SCNPs with that of disordered proteins [19,96]. Analyzing the size reductions observed for reversibly crosslinked systems revealed that chain collapse in these systems is on average smaller than in covalently crosslinked SCNPs [81]. This is of advantage in the efforts towards protein mimicry, as the collapse of supramolecularly crosslinked SCNPs allows for the formation of pockets, similar as encountered in proteins that contain active sites or anchoring pockets. Substrates can anchor in these pockets and interact

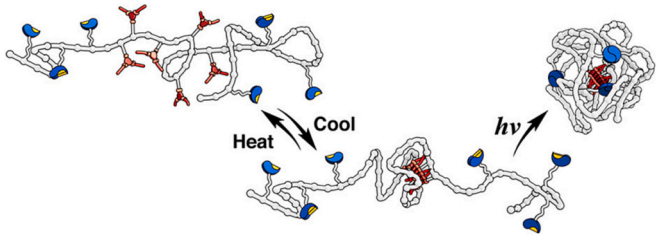

Fig. 12. Illustration of SCNP folding of a ABA block *co*-polymer with sequential folding motifs. Reproduced with permission from ref. [24] with permission of American Chemical Society (2013).

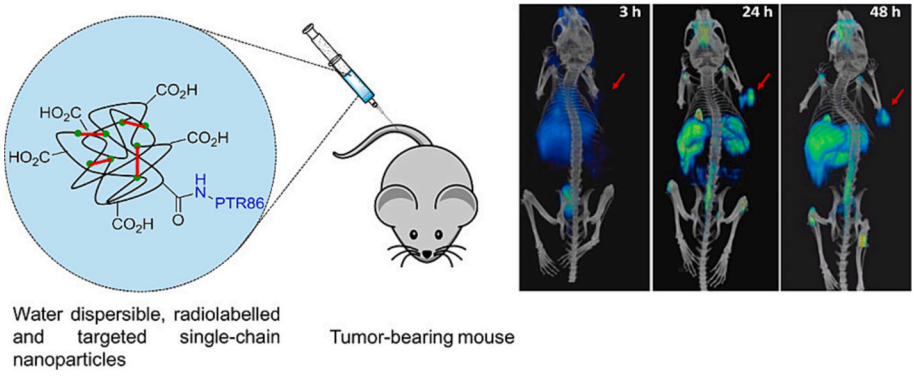

Fig. 11. SPECT-CT images of pancreatic tumor-bearing mice injected with PTR86 conjugated radiolabeled SCNPs recorded 3, 24 and 48 h after injection. The red arrows indicate the tumor site. Adapted from ref. [37] with permission of American Chemical Society (2016). (For interpretation of the references to colour in this figure legend, the reader is referred to the web version of this article.)

with the catalyst to either be cleaved or react with a second substrate, resembling the function of enzymes.

For proteins such as actin, functionality is not only based on the folding of the molecule itself, but additionally on the interactions and stacking of multiple molecules to form filaments. In order to simulate this interaction, self-assembly of SCNPs has been studied by Wen et al., utilizing crosslinked SCNPs with a hydrophobic core and hydrophilic tail [115]. The formation of tubular and spherical structures was observed, depending on the degree of crosslinking in the SCNPs and the molecular weight of the hydrophilic tail (see Fig. 13). Larger particle formation utilizing SCNPs has been shown by Song et al. as described in Section 6.4 SCNPs in controlled drug delivery [18]. Reversible aggregation of SCNPs into larger NPs can lead to improved properties for biomedical application. Controlling the shape of these larger particles will further influence the interactions with cells, as particle shape has been shown to be a key property involved in cellular uptake and biodistribution [116,117].

SCNPs typically span the 5–20 nm size range, which matches the sizes of many proteins. In an approach that mimics proteins with respect to their size and surface functionality, the Paulusse group developed protein mimics using covalently crosslinked SCNPs with activated pentafluorophenyl esters [40]. The activated esters were demonstrated to be readily substituted with a wide range of functional amines, even at different incorporation ratios, while maintain the core particle unaltered. Amino acids such as alanine and tyrosine were conjugated, but also small peptides such as glutathione and even hexahistidine (His_6) peptide. Successful functionalization was confirmed by ^{1}H and ^{19}F NMR spectroscopy. Interestingly, His_6-labeled SCNPs showed affinity with nickel-nitrilotriacetic acid columns, as the SCNPs were only released upon elution with imidazole containing buffer. These results showed that the His_6-peptide was intact after conjugation onto SCNPs, establishing successful formation of active SCNP-protein hybrids, with important opportunities for mimicking proteins more closely.

As research is progressing towards higher resemblance with proteins, research into partial denaturing of BSA molecules was conducted to obtain polypeptides for SCNP formation [118]. The partially denatured BSA coil contained disulfide bonds and additional covalent crosslinks were introduced. Small-angle neutron scattering was utilized to measure the changes in the structure of BSA from the globular BSA to a random coil in the denatured state and the shrinkage upon SCNPs formation. This strategy enables the use of polypeptides as backbones for SCNP formation. The synthesis of peptides as polymer backbones for SCNP formation is still challenging, however, due to the high molecular weights required for successful SCNP formation. Future advances in peptide synthesis may lead to additional potential for synthetic peptides in SCNP formation. However, the strategies of protein mimicry introduced in SCNP research including SCNP functionalization using peptides, and protein denaturation and further crosslinking have shown promising results to be further explored in the future.

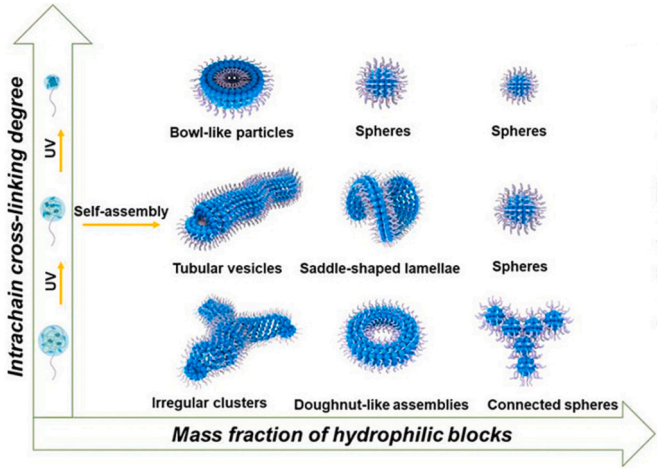

Fig. 13. Scheme of 3D structures formed by self-assembly of SCNPs dependent on crosslinking degree and hydrophilic/hydrophobic block ratios in selective solvent. Adapted from ref. [110] with permission of American Chemical Society (2019).

6.8. *Enzyme mimicry*

Enzymes are an interesting class of catalysts, as they function in water under mild conditions and at neutral pH. These properties make enzymes attractive for applications in agriculture and food production [119]. In the field of biomedical applications enzyme mimicry is explored in view of more efficiently combating diseases, such as enzyme replacement therapy [120] and cancer therapy [121,122]. Enzyme mimicry has multiple functions that have to be addressed, including the recognition of specific substrates, the catalysis of selected reactions and the recyclability of enzymes [119]. SCNPs form a great platform for enzyme mimicry, as the controlled folded structures allow for easy integration of catalysts into their structure to enhance stability, selectivity and even recyclability. In the previous paragraph we have discussed the ability of SCNPs to form anchoring pockets for substrates. Here, we will focus on the progress of SCNP enzyme mimicry in the catalysis reactions. In the work of Pomposo and co-workers, SCNPs were crosslinked by Cu(II) complexation [34,67] and later Fe(II) complexation [13]. The nanoreactors showed increased stability against thermal changes as well as higher specificity at low Cu(II) concentrations as compared to classical catalysts. Higher catalytic efficiency of SCNPs containing Cu(II) was achieved by clustering Cu(II) ions in the SCNPs, reaching a yield of 95% as compared to a 65% yield for SCNPs with homogenously distributed Cu(II) ions [26]. Aiming at biomedical application of catalytically active SCNPs, cellular uptake of Cu(II) containing nanoreactors by human non-small cell lung carcinoma (NCI-H460) and human breast cancer cells (MD-MB-231) was assessed [104]. After 1 h incubation of the nanoreactors, the cells were washed and a substrate for azide-alkyne cycloaddition, alongside sodium ascorbate, was added to the cells. The cells incubated with the nanoreactor expressed a strong fluorescent signal, evident for a successful intracellular click reaction occurring. The intracellular activity of SCNPs with Cu(I) or Pd(II) in HeLa cells was also studied by Liu et al. [22], presenting superior catalytic activity in SCNPs as compared to the free catalyst. Further research into the use of SCNPs as nanoreactors for Cu-click reactions, involved the synthesis of polyacrylamide-based SCNPs containing tris(triazolylmethyl)amine units as Cu(I) ligand [31]. These SCNPs have shown recyclability of the catalyst and have the ability to adaptively and reversibly bind to protein surfaces. Cell membrane labeling was thereby shown on non-small-cell lung cancer cells (H460 cells). The cells were incubated with Ac4ManNaI or Ac4ManNAz to integrate alkyne or azide units on the cell surface glycans (see Fig. 14a). Subsequently, the alkyne functionalized cells were incubated with coumarin azide, whereas azide functionalized cells were incubated with alkynylated fluorescent mCherry. Incubation with Cu(I)-SCNPs showed a higher degree of cell membrane labeling compared to Cu(I)-BTGTA (see Fig. 14).

To achieve extracellular CuAAC reactions, SCNPs were prepared with PEG functionalities on the surface [45]. The CuAAC reaction with Cu(I) containing PEG-SCNPs to couple alkyne-functional small molecules (4-ethynylanisole) or proteins (bovine serum albumin) with fluorescent 3-azido-7-hydroxy-coumarin was compared to SCNPs containing cationic surface groups [31]. Both SCNPs showed efficient click reactions with high conversions within 5 min for the small molecule reaction [45]. However, when the click reaction was executed with an alkynylated protein a 137-fold lower reaction rate was observed for the PEG-SCNPs, indicating that the PEG-coated particle surface prevents the protein from binding to active sites on the SCNPs. The SCNPs with PEG functionalization display only minor fluorescence in HeLa cells as

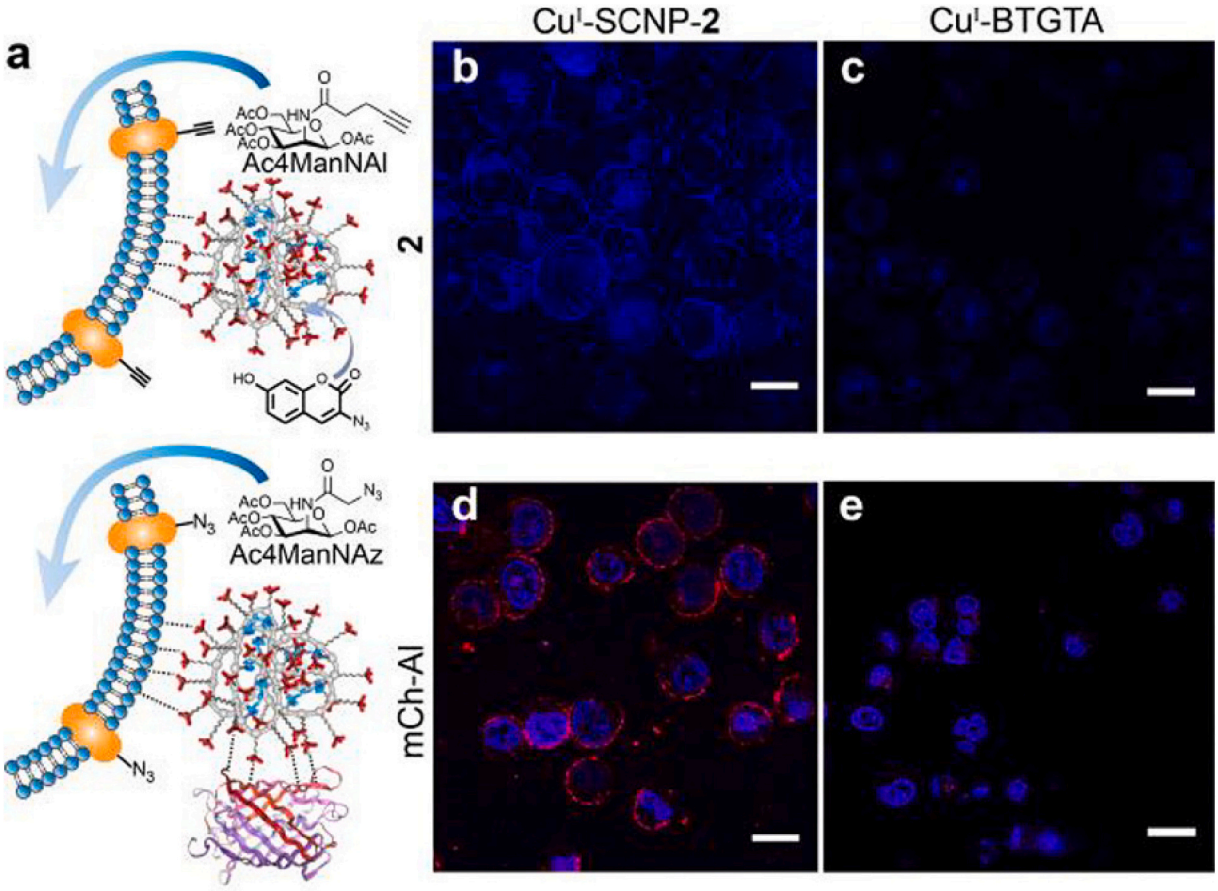

Fig. 14. Cell labeling utilizing C(I)-SCNPs a) Illustration of metabolic labeling of cell surface glycans utilizing mannose derivates with either an azido or alkyne functionality and Cu(I)-SCNP; Confocal images of H460 cells incubated with Cu(I)-SCNPs (1 μM) (b), or Cu(I)-BTGTA (10 μM) (c), coumarin azide (100 μM) and sodium ascorbate (2 mM) in PBS buffer for 30 min. Confocal images of H460 cells incubated with Cu(I)-SCNPs (1 μM) (d) or Cu(I)-BTGTA (10 μM) (e), alkynylated mCherry (1 μM) and sodium ascorbate (2 mM) in PBS buffer for 30 min. The nuclei were stained in blue in (d) and (e), scale bar 20 μm. Reproduced with permission from ref. [31] with permission of American Chemical Society (2019). (For interpretation of the references to colour in this figure legend, the reader is referred to the web version of this article.)

compared to the SCNPs containing quaternary amines. Further studies confirmed a successful CuAAC reaction extracellularly of the HeLa cells (see Fig. 15), while the fluorescent product rapidly diffuses into the cell, reaching maximum signal after 10 min.

Terashima et al. developed self-folding SCNPs with a hydrophobic core to host a catalyst [12]. Introduction of benzene-1,3,5-tricarboxamide side-chains led to the formation of helical structures in the hydrophobic core, which was equipped with Ru-complexes. Folding of these SCNPs resembles to certain extents that of proteins, while in this case also catalytic activity was integrated. The metal-ligand coordination bonds formed in the SCNPs stabilize polymer folding, while providing catalytic activity. [58]

Liu et al. developed supramolecularly crosslinked SCNPs bearing porphyrins, which produce singlet oxygen ($^1O_2$) upon photoirradiation and therefore have an application in photodynamic therapy [32]. The porphyrin conjugated SCNPs were incubated at different concentrations with HeLa cells [22]. Cellular uptake was confirmed by CLSM and activation of the porphyrin SCNPs was achieved by irradiation at 403 nm. Significant cell death was observed with a live/dead assay as compared to SCNPs without porphyrin. Further evaluations into the effects of concentration and irradiation times showed decreases in viability starting at a concentration of 100 μg/mL and an irradiation time of 150 s, while cell death was induced at a concentration of 500 μg/mL when irradiated for 30 s.

Intracellular activation of anti-cancer agents through a dual approach was shown by Chen et al., who used SCNPs containing tris (bipyridine) ruthenium ($Ru(bpy)_3$) (i.e. Ru-SCNPs) together with β-galactosidase (βGal) [23]. HeLa cells were incubated with Ru-SCNPs, in conjunction with βGal and two prodrugs, i.e. a DOX derivate and galactose-masked combretastastin A4. Upon activation of the nanoreactor via irradiation at 470 nm for 5 min, significant cell death was observed. Although incubation with each individual prodrug showed similar decreases in cell viability (>60%), the combination of both prodrugs led to a further decrease in cell viability to below 20%, as shown in Fig. 16. Application of SCNPs as nanoreactors in photodynamic therapy highlights the possibility of decreasing cancer cell viability. However, prodrugs need to be incubated with the cells in order to achieve this effect, which for application in vivo would require co-delivery of both nanoreactors and prodrugs to a specific target region in the body.

Research in the field of enzyme mimicry has led to promising results, as the SCNPs have the ability to both act as a delivery system for catalytically active species, as well as providing stability leading to high efficiency catalysts in biological environments.

7. Conclusions

This review has provided an overview of the growing synthetic toolbox developed for SCNP formation. Polymer chemistry has been utilized to broaden the crosslinking strategies and functionalization of SCNPs. This has led to tremendous progress in application-based research. To reach uniform SCNPs, low polydispersity of the precursor

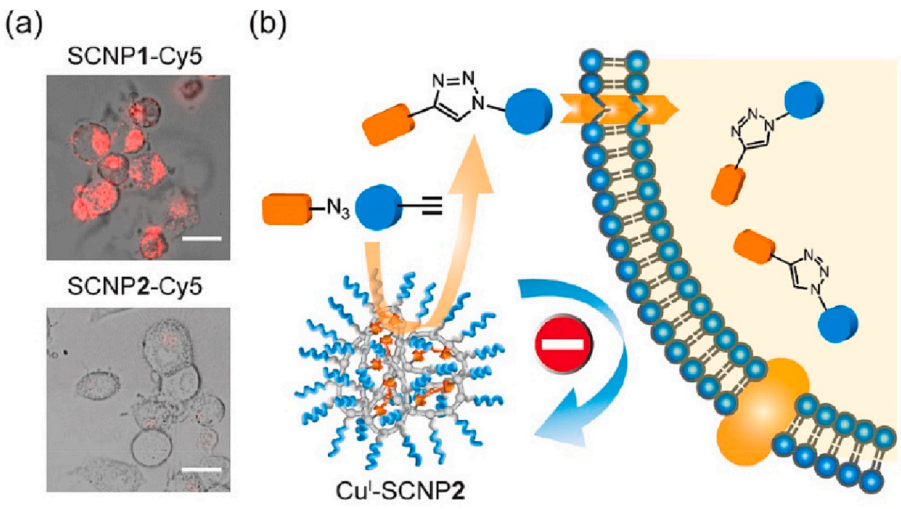

Fig. 15. a) Confocal images of HeLa cells incubated with PEGylated SCNP or SCNP (SCNP1) with cationic surface charges (SCNP2); b) Illustration of extracellular CuAAC synthesis and diffusion across cell membrane of reaction product; c) Confocal images of HeLa cells in PBS buffer in blue is the fluorescent product of the extracellular synthesis catalyzed by Cu (I) containing PEGylated SCNPs. Reproduced with permission from ref. [45] with permission of American Chemical Society (2020). (For interpretation of the references to colour in this figure legend, the reader is referred to the web version of this article.)

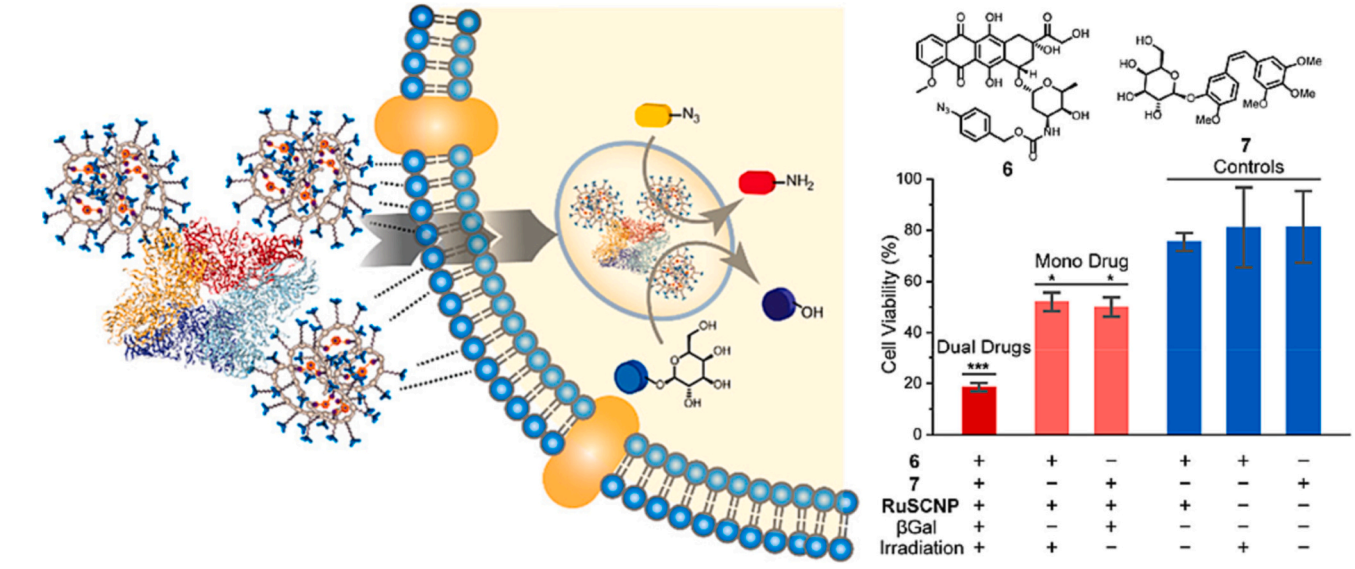

Fig. 16. Illustration of SCNP- βGal tandem delivery and catalysis; b) Viability of Hela cells after incubation with various combinations of substrates 6 (1 μM) and 7 (4 μM), Ru-SCNPs (200 nM), βGal (20 nM) and irradiation at 470 nm for 5 min measured by MTT assay. Error bars consist of standard deviation of three independent runs. Adapted from ref. [23] with permission of American Chemical Society (2020).

polymer is required, which can be achieved by controlled polymerization techniques. Targeting of specific cell lines and subcellular location has been explored. Further research in optimization of the surface chemistry of SCNPs to enable weak multivalent interactions with cell receptors will provide selective and enhanced cellular uptake. In controlled drug delivery, SCNPs have been studied for their ability to encapsulate and release therapeutics. Next to drug encapsulation, which has also been shown to affect particle size in some SCNP systems, drug conjugation may offer another promising route. Additionally, antibacterial behavior of SCNPs has been studied, revealing enhanced activity

for SCNPs containing high charge density and hydrophobicity. The combination of targeting ligands with an antibacterial SCNP structure and encapsulated antibiotics, may give powerful bactericidal agents. In the future, the advantages of SCNPs in comparison to other nanoparticles for specific applications should be investigated to better assess the optimal potential of SCNPs. Detailed investigations into sequential and controlled polymer folding has already given valuable insights into the resemblance with protein folding. Successful integration of various catalysts has been shown, while SCNPs can even provide improved catalytic activity as shown in certain biological environments. This has led to the first applications of SCNPs in photodynamic therapy in in vitro studies. A key property of nanocarriers for biomedical application is biocompatibility. SCNPs have shown convincing results in in vitro studies, maintaining good cell viabilities, which is only reduced by specific toxicity of certain functional groups. In the future, systematic investigations into biocompatibility, biodistribution and behavior of the SCNPs in their denoted application are required to reveal the full potential of SCNPs for in vivo applications. In the future, systematic investigations into biocompatibility, biodistribution and behavior of the SCNPs in their denoted application are required to reveal the full potential of SCNPs for in vivo applications.

CRediT authorship contribution statement

Naomi M. Hamelmann: Conceptualization, Writing – original draft, Visualization. **Jos M.J. Paulusse:** Conceptualization, Writing – review & editing, Supervision, Visualization, Project administration, Funding acquisition.

Data availability

No data was used for the research described in the article.

References

[1] G. Moad, C. Barner-Kowollik, The mechanism and kinetics of the RAFT process: overview, rates, stabilities, side reactions, product spectrum and outstanding challenges, in: Handbook of RAFT Polymerization, 2008, pp. 51–104.

[2] W.A. Braunecker, K. Matyjaszewski, Controlled/living radical polymerization: features, developments, and perspectives, Prog. Polym. Sci. 32 (1) (2007) 93–146.

[3] O. Galant, H.B. Donmez, C. Barner-Kowollik, C.E. Diesendruck, Flow photochemistry for single-chain polymer nanoparticle synthesis, Angew. Chem. Int. Ed. 60 (4) (2021) 2042–2046.

[4] C.-C. Cheng, F.-C. Chang, H.-C. Yen, D.-J. Lee, C.-W. Chiu, Z. Xin, Supramolecular assembly mediates the formation of single-chain polymeric nanoparticles, ACS Macro Lett. 4 (10) (2015) 1184–1188.

[5] J. Willenbacher, K.N.R. Wuest, J.O. Mueller, M. Kaupp, H.-A. Wagenknecht, C. Barner-Kowollik, Photochemical design of functional fluorescent single-chain nanoparticles, ACS Macro Lett. 3 (6) (2014) 574–579.

[6] N. Ormategui, I. García, D. Padro, G. Cabañero, H.J. Grande, I. Loinaz, Synthesis of single chain thermoresponsive polymer nanoparticles, Soft Matter 8 (3) (2012) 734–740.

[7] R. Gracia, M. Marradi, U. Cossío, A. Benito, A. Pérez-San Vicente, V. Gómez-Vallejo, H.J. Grande, J. Llop, I. Loinaz, Synthesis and functionalization of dextran-based single-chain nanoparticles in aqueous media, J. Mater. Chem. B 5 (6) (2017) 1143–1147.

[8] A.P.P. Kröger, R.J.E.A. Boonen, J.M.J. Paulusse, Well-defined single-chain polymer nanoparticles via thiol-Michael addition, Polymer 120 (2017) 119–128.

[9] I. Perez-Baena, I. Loinaz, D. Padro, I. García, H.J. Grande, I. Odriozola, Single-chain polyacrylic nanoparticles with multiple Gd(iii) centres as potential MRI contrast agents, J. Mater. Chem. 20 (33) (2010) 6916–6922.

[10] A.P.P. Kröger, N.M. Hamelmann, A. Juan, S. Lindhoud, J.M.J. Paulusse, Biocompatible single-chain polymer nanoparticles for drug delivery—a dual approach, ACS Appl. Mater. Interfaces 10 (37) (2018) 30946–30951.

[11] J.B. Beck, K.L. Killops, T. Kang, K. Sivanandan, A. Bayles, M.E. Mackay, K. L. Wooley, C.J. Hawker, Facile preparation of nanoparticles by intramolecular cross-linking of isocyanate functionalized copolymers, Macromolecules 42 (15) (2009) 5629–5635.

[12] T. Terashima, T. Mes, T.F.A. De Greef, M.A.J. Gillissen, P. Besenius, A.R. A. Palmans, E.W. Meijer, Single-chain folding of polymers for catalytic systems in water, J. Am. Chem. Soc. 133 (13) (2011) 4742–4745.

[13] J. De-La-Cuesta, I. Asenjo-Sanz, A. Latorre-Sánchez, E. González, D.E. Martínez-Tong, J.A. Pomposo, Enzyme-mimetic synthesis of PEDOT from self-folded iron-containing single-chain nanoparticles, Eur. Polym. J. 109 (2018) 447–452.

[14] J. Engelke, J. Brandt, C. Barner-Kowollik, A. Lederer, Strengths and limitations of size exclusion chromatography for investigating single chain folding – current status and future perspectives, Polym. Chem. 10 (25) (2019) 3410–3425.

[15] J. Engelke, B.T. Tuten, R. Schweins, H. Komber, L. Barner, L. Plüschke, C. Barner-Kowollik, A. Lederer, An in-depth analysis approach enabling precision single chain nanoparticle design, Polym. Chem. 11 (41) (2020) 6559–6578.

[16] E. Blasco, B.T. Tuten, H. Frisch, A. Lederer, C. Barner-Kowollik, Characterizing single chain nanoparticles (SCNPs): a critical survey, Polym. Chem. 8 (38) (2017) 5845–5851.

[17] C.-C. Cheng, S.-Y. Huang, W.-L. Fan, A.-W. Lee, C.-W. Chiu, D.-J. Lee, J.-Y. Lai, Water-soluble single-chain polymeric nanoparticles for highly selective cancer chemotherapy, ACS Appl. Polym. Mater. 3 (1) (2021) 474–484.

[18] C. Song, T. Lin, Q. Zhang, S. Thayumanavan, L. Ren, pH-sensitive morphological transitions in polymeric tadpole assemblies for programmed tumor therapy, J. Control. Release 293 (2019) 1–9.

[19] A. Sanchez-Sanchez, S. Akbari, A. Etxeberria, A. Arbe, U. Gasser, A.J. Moreno, J. Colmenero, J.A. Pomposo, "Michael" nanocarriers mimicking transient-binding disordered proteins, ACS Macro Lett. 2 (6) (2013) 491–495.

[20] T.-K. Nguyen, S.J. Lam, K.K.K. Ho, N. Kumar, G.G. Qiao, S. Egan, C. Boyer, E.H. H. Wong, Rational design of single-chain polymeric nanoparticles that kill planktonic and biofilm bacteria, ACS Infect. Dis. 3 (3) (2017) 237–248.

[21] X. Tian, R. Xue, F. Yang, L. Yin, S. Luan, H. Tang, Single-chain nanoparticle-based coatings with improved bactericidal activity and antifouling properties, Biomacromolecules 22 (10) (2021) 4306–4315.

[22] Y. Liu, S. Pujals, P.J.M. Stals, T. Paulöhrl, S.I. Presolski, E.W. Meijer, L. Albertazzi, A.R.A. Palmans, Catalytically active single-chain polymeric nanoparticles: exploring their functions in complex biological media, J. Am. Chem. Soc. 140 (9) (2018) 3423–3433.

[23] J. Chen, K. Li, J.S.L. Shon, S.C. Zimmerman, Single-chain nanoparticle delivers a partner enzyme for concurrent and tandem catalysis in cells, J. Am. Chem. Soc. 142 (10) (2020) 4565–4569.

[24] N. Hosono, M.A.J. Gillissen, Y. Li, S.S. Sheiko, A.R.A. Palmans, E.W. Meijer, Orthogonal self-assembly in folding block copolymers, J. Am. Chem. Soc. 135 (1) (2013) 501–510.

[25] H. Frisch, D. Kodura, F.R. Bloesser, L. Michalek, C. Barner-Kowollik, Wavelength-selective folding of single polymer chains with different colors of visible light, Macromol. Rapid Commun. 41 (1) (2020) 1900414.

[26] I. Asenjo-Sanz, T. Claros, E. González, J. Pinacho-Olaciregui, E. Verde-Sesto, J. A. Pomposo, Significant effect of intra-chain distribution of catalytic sites on catalytic activity in "clickase" single-chain nanoparticles, Mater. Lett. 304 (2021), 130622.

[27] M.A.M. Alqarni, C. Waldron, G. Yilmaz, C.R. Becer, Synthetic routes to single chain polymer nanoparticles (SCNPs): current status and perspectives, Macromol. Rapid Commun. 42 (11) (2021) 2100035.

[28] A.P.P. Kröger, J.M.J. Paulusse, Single-chain polymer nanoparticles in controlled drug delivery and targeted imaging, J. Control. Release 286 (2018) 326–347.

[29] S. Mavila, O. Eivgi, I. Berkovich, N.G. Lemcoff, Intramolecular cross-linking methodologies for the synthesis of polymer nanoparticles, Chem. Rev. 116 (3) (2016) 878–961.

[30] E. Harth, B.V. Horn, V.Y. Lee, D.S. Germack, C.P. Gonzales, R.D. Miller, C. J. Hawker, A facile approach to architecturally defined nanoparticles via intramolecular chain collapse, J. Am. Chem. Soc. 124 (29) (2002) 8653–8660.

[31] J. Chen, J. Wang, K. Li, Y. Wang, M. Gruebele, A.L. Ferguson, S.C. Zimmerman, Polymeric "clickase" accelerates the copper click reaction of small molecules, proteins, and cells, J. Am. Chem. Soc. 141 (24) (2019) 9693–9700.

[32] Y. Liu, T. Pauloehrl, S.I. Presolski, L. Albertazzi, A.R.A. Palmans, E.W. Meijer, Modular synthetic platform for the construction of functional single-chain polymeric nanoparticles: from aqueous catalysis to photosensitization, J. Am. Chem. Soc. 137 (40) (2015) 13096–13105.

[33] C.-C. Cheng, D.-J. Lee, Z.-S. Liao, J.-J. Huang, Stimuli-responsive single-chain polymeric nanoparticles towards the development of efficient drug delivery systems, Polym. Chem. 7 (40) (2016) 6164–6169.

[34] A. Sanchez-Sanchez, A. Arbe, J. Colmenero, J.A. Pomposo, Metallo-folded single-chain nanoparticles with catalytic selectivity, ACS Macro Lett. 3 (5) (2014) 439–443.

[35] S.K. Hamilton, E. Harth, Molecular dendritic transporter nanoparticle vectors provide efficient intracellular delivery of peptides, ACS Nano 3 (2) (2009) 402–410.

[36] A. Sanchez-Sanchez, D.A. Fulton, J.A. Pomposo, pH-responsive single-chain polymer nanoparticles utilising dynamic covalent enamine bonds, Chem. Commun. 50 (15) (2014) 1871–1874.

[37] A.B. Benito, M.K. Aiertza, M. Marradi, L. Gil-Iceta, T. Shekhter Zahavi, B. Szczupak, M. Jiménez-González, T. Reese, E. Scanziani, L. Passoni, M. Matteoli, M. De Maglie, A. Orenstein, M. Oron-Herman, G. Kostenich, L. Buzhansky, E. Gazit, H.-J. Grande, V. Gómez-Vallejo, J. Llop, I. Loinaz, Functional single-chain polymer nanoparticles: targeting and imaging pancreatic tumors in vivo, Biomacromolecules 17 (10) (2016) 3213–3221.

[38] J.É.F. Radu, L. Novak, J.F. Hartmann, N. Beheshti, A.-L. Kjøniksen, B. Nyström, J. Borbély, Structural and dynamical characterization of poly-gamma-glutamic acid-based cross-linked nanoparticles, Colloid Polym. Sci. 286 (4) (2008) 365–376.

[39] D.E. Whitaker, C.S. Mahon, D.A. Fulton, Thermoresponsive dynamic covalent single-chain polymer nanoparticles reversibly transform into a hydrogel, Angew. Chem. Int. Ed. 52 (3) (2013) 956–959.

[40] A.P.P. Kröger, J.-W.D. Paats, R.J.E.A. Boonen, N.M. Hamelmann, J.M.J. Paulusse, Pentafluorophenyl-based single-chain polymer nanoparticles as a versatile platform towards protein mimicry, Polym. Chem. 11 (37) (2020) 6056–6065.
[41] R. Gracia, M. Marradi, G. Salerno, R. Pérez-Nicado, A. Pérez-San Vicente, D. Dupin, J. Rodriguez, I. Loinaz, F. Chiodo, C. Nativi, Biocompatible single-chain polymer nanoparticles loaded with an antigen mimetic as potential anticancer vaccine, ACS Macro Lett. 7 (2) (2018) 196–200.
[42] Y. Zhang, H. Zhao, Surface-tunable colloidal particles stabilized by mono-tethered single-chain nanoparticles, Polymer 64 (2015) 277–284.
[43] L. Zhao, X. Wang, L. Sun, R. Zhou, X. Zhang, L. Zhang, Z. Zheng, Y. Ling, S. Luan, H. Tang, Synthesis and UCST-type thermoresponsive properties of polypeptide based single-chain nanoparticles, Polym. Chem. 10 (38) (2019) 5206–5214.
[44] A.R. de Luzuriaga, N. Ormategui, H.J. Grande, I. Odriozola, J.A. Pomposo, I. Loinaz, Intramolecular click cycloaddition: an efficient room-temperature route towards bioconjugable polymeric nanoparticles, Macromol. Rapid Commun. 29 (12–13) (2008) 1156–1160.
[45] J. Chen, K. Li, S.E. Bonson, S.C. Zimmerman, A bioorthogonal small molecule selective polymeric "clickase", J. Am. Chem. Soc. 142 (32) (2020) 13966–13973.
[46] J. Maiz, E. Verde-Sesto, I. Asenjo-Sanz, P. Fouquet, L. Porcar, J.A. Pomposo, P. M. de Molina, A. Arbe, J. Colmenero, Collective motions and mechanical response of a bulk of single-chain nano-particles synthesized by click-chemistry, Polymers 13 (1) (2021) 50.
[47] K.N.R. Wuest, H. Lu, D.S. Thomas, A.S. Goldmann, M.H. Stenzel, C. Barner-Kowollik, Fluorescent glyco single-chain nanoparticle-decorated nanodiamonds, ACS Macro Lett. 6 (10) (2017) 1168–1174.
[48] J.T. Offenloch, J. Willenbacher, P. Tzvetkova, C. Heiler, H. Mutlu, C. Barner-Kowollik, Degradable fluorescent single-chain nanoparticles based on metathesis polymers, Chem. Commun. 53 (4) (2017) 775–778.
[49] C. Heiler, J.T. Offenloch, E. Blasco, C. Barner-Kowollik, Photochemically induced folding of single chain polymer nanoparticles in water, ACS Macro Lett. 6 (1) (2017) 56–61.
[50] H. Zhang, L. Zhang, J. You, N. Zhang, L. Yu, H. Zhao, H.J. Qian, Z.Y. Lu, Controlling the chain folding for the synthesis of single-chain polymer nanoparticles using thermoresponsive polymers, CCS Chem. 3 (8) (2021) 2143–2154.
[51] S. Mura, J. Nicolas, P. Couvreur, Stimuli-responsive nanocarriers for drug delivery, Nat. Mater. 12 (11) (2013) 991–1003.
[52] W. Fan, X. Tong, Q. Yan, S. Fu, Y. Zhao, Photodegradable and size-tunable single-chain nanoparticles prepared from a single main-chain coumarin-containing polymer precursor, Chem. Commun. 50 (88) (2014) 13492–13494.
[53] C. Song, L. Li, L. Dai, S. Thayumanavan, Responsive single-chain polymer nanoparticles with host–guest features, Polym. Chem. 6 (26) (2015) 4828–4834.
[54] H. Mutlu, C. Barner-Kowollik, Green chain-shattering polymers based on a self-immolative azobenzene motif, Polym. Chem. 7 (12) (2016) 2272–2279.
[55] J.M.J. Paulusse, R.J. Amir, R.A. Evans, C.J. Hawker, Free radical polymers with tunable and selective bio- and chemical degradability, J. Am. Chem. Soc. 131 (28) (2009) 9805–9812.
[56] A.W. Jackson, L.R. Chennamaneni, S.R. Mothe, P. Thoniyot, A general strategy for degradable single-chain nanoparticles via cross-linker mediated chain collapse of radical copolymers, Chem. Commun. 56 (68) (2020) 9838–9841.
[57] M. Seo, B.J. Beck, J.M.J. Paulusse, C.J. Hawker, S.Y. Kim, Polymeric nanoparticles via noncovalent cross-linking of linear chains, Macromolecules 41 (17) (2008) 6413–6418.
[58] M. Artar, T. Terashima, M. Sawamoto, E.W. Meijer, A.R.A. Palmans, Understanding the catalytic activity of single-chain polymeric nanoparticles in water, J. Polym. Sci. A Polym. Chem. 52 (1) (2014) 12–20.
[59] Y. Abdouni, G.M. ter Huurne, G. Yilmaz, A. Monaco, C. Redondo-Gómez, E. W. Meijer, A.R.A. Palmans, C.R. Becer, Self-assembled multi- and single-chain glyconanoparticles and their lectin recognition, Biomacromolecules 22 (2) (2021) 661–670.
[60] Y. Liu, P. Turunen, B.F.M. de Waal, K.G. Blank, A.E. Rowan, A.R.A. Palmans, E. W. Meijer, Catalytic single-chain polymeric nanoparticles at work: from ensemble towards single-particle kinetics, Mol. Syst. Des. Eng. 3 (4) (2018) 609–618.
[61] L. Deng, L. Albertazzi, A.R.A. Palmans, Elucidating the stability of single-chain polymeric nanoparticles in biological media and living cells, Biomacromolecules 23 (1) (2022) 326–338.
[62] K. Matsumoto, T. Terashima, T. Sugita, M. Takenaka, M. Sawamoto, Amphiphilic random copolymers with hydrophobic/hydrogen-bonding urea pendants: self-folding polymers in aqueous and organic media, Macromolecules 49 (20) (2016) 7917–7927.
[63] E.J. Foster, E.B. Berda, E.W. Meijer, Metastable supramolecular polymer nanoparticles via intramolecular collapse of single polymer chains, J. Am. Chem. Soc. 131 (20) (2009) 6964–6966.
[64] E.J. Foster, E.B. Berda, E.W. Meijer, Tuning the size of supramolecular single-chain polymer nanoparticles, J. Polym. Sci. A Polym. Chem. 49 (1) (2011) 118–126.
[65] T. Terashima, T. Sugita, K. Fukae, M. Sawamoto, Synthesis and single-chain folding of amphiphilic random copolymers in water, Macromolecules 47 (2) (2014) 589–600.
[66] S.-Y. Huang, C.-C. Cheng, Spontaneous self-assembly of single-chain amphiphilic polymeric nanoparticles in water, Nanomaterials 10 (10) (2020) 2006.
[67] A. Sanchez-Sanchez, A. Arbe, J. Kohlbrecher, J. Colmenero, J.A. Pomposo, Efficient synthesis of single-chain globules mimicking the morphology and polymerase activity of metalloenzymes, Macromol. Rapid Commun. 36 (17) (2015) 1592–1597.
[68] D. Chao, X. Jia, B. Tuten, C. Wang, E.B. Berda, Controlled folding of a novel electroactive polyolefin via multiple sequential orthogonal intra-chain interactions, Chem. Commun. 49 (39) (2013) 4178–4180.
[69] A.M. Hanlon, C.K. Lyon, E.B. Berda, What is next in single-chain nanoparticles? Macromolecules 49 (1) (2016) 2–14.
[70] A.M. Hanlon, R. Chen, K.J. Rodriguez, C. Willis, J.G. Dickinson, M. Cashman, E. B. Berda, Scalable synthesis of single-chain nanoparticles under mild conditions, Macromolecules 50 (7) (2017) 2996–3003.
[71] E.H.H. Wong, G.G. Qiao, Factors influencing the formation of single-chain polymeric nanoparticles prepared via ring-opening polymerization, Macromolecules 48 (5) (2015) 1371–1379.
[72] E. Blasco, M.B. Sims, A.S. Goldmann, B.S. Sumerlin, C. Barner-Kowollik, 50th anniversary perspective: polymer functionalization, Macromolecules 50 (14) (2017) 5215–5252.
[73] A. Gruber, L. Navarro, D. Klinger, Reactive precursor particles as synthetic platform for the generation of functional nanoparticles, nanogels, and microgels, Adv. Mater. Interfaces 7 (5) (2020) 1901676.
[74] M.A. Gauthier, M.I. Gibson, H.-A. Klok, Synthesis of functional polymers by post-polymerization modification, Angew. Chem. Int. Ed. 48 (1) (2009) 48–58.
[75] J. Chen, J. Wang, K. Li, Y. Wang, M. Gruebele, A.L. Ferguson, S.C. Zimmerman, Polymeric "clickase" accelerates the copper click reaction of small molecules, proteins, and cells, J. Am. Chem. Soc. 141 (24) (2019) 9693–9700.
[76] N.M. Hamelmann, J.-W.D. Paats, J.M.J. Paulusse, Cytosolic delivery of single-chain polymer nanoparticles, ACS Macro Lett. (2021) 1443–1449.
[77] Y. Bai, H. Xing, P. Wu, X. Feng, K. Hwang, J.M. Lee, X.Y. Phang, Y. Lu, S. C. Zimmerman, Chemical control over cellular uptake of organic nanoparticles by fine tuning surface functional groups, ACS Nano 9 (10) (2015) 10227–10236.
[78] G. Arias-Alpizar, B. Koch, N.M. Hamelmann, M.A. Neustrup, J.M.J. Paulusse, W. Jiskoot, A. Kros, J. Bussmann, Stabilin-1 is required for the endothelial clearance of small anionic nanoparticles, Nanomed. Nanotechnol. Biol. Med. 34 (2021), 102395.
[79] K.M. Tsoi, S.A. MacParland, X.-Z. Ma, V.N. Spetzler, J. Echeverri, B. Ouyang, S. M. Fadel, E.A. Sykes, N. Goldaracena, J.M. Kaths, J.B. Conneely, B.A. Alman, M. Selzner, M.A. Ostrowski, O.A. Adeyi, A. Zilman, I.D. McGilvray, W.C.W. Chan, Mechanism of hard-nanomaterial clearance by the liver, Nat. Mater. 15 (11) (2016) 1212–1221.
[80] A.H. Bahrami, M. Raatz, J. Agudo-Canalejo, R. Michel, E.M. Curtis, C.K. Hall, M. Gradzielski, R. Lipowsky, T.R. Weikl, Wrapping of nanoparticles by membranes, Adv. Colloid Interf. Sci. 208 (2014) 214–224.
[81] J.A. Pomposo, J. Rubio-Cervilla, A.J. Moreno, F. Lo Verso, P. Bacova, A. Arbe, J. Colmenero, Folding single chains to single-chain nanoparticles via reversible interactions: what size reduction can one expect? Macromolecules 50 (4) (2017) 1732–1739.
[82] X. Chen, R. Li, S.H.D. Wong, K. Wei, M. Cui, H. Chen, Y. Jiang, B. Yang, P. Zhao, J. Xu, H. Chen, C. Yin, S. Lin, W.Y.-W. Lee, Y. Jing, Z. Li, Z. Yang, J. Xia, G. Chen, G. Li, L. Bian, Conformational manipulation of scale-up prepared single-chain polymeric nanogels for multiscale regulation of cells, Nat. Commun. 10 (1) (2019) 2705.
[83] J.A. Pomposo, I. Perez-Baena, F. Lo Verso, A.J. Moreno, A. Arbe, J. Colmenero, How far are single-chain polymer nanoparticles in solution from the globular state? ACS Macro Lett. 3 (8) (2014) 767–772.
[84] H. Hofmann, A. Soranno, A. Borgia, K. Gast, D. Nettels, B. Schuler, Polymer scaling laws of unfolded and intrinsically disordered proteins quantified with single-molecule spectroscopy, Proc. Natl. Acad. Sci. 109 (40) (2012) 16155–16160.
[85] J.A. Marsh, J.D. Forman-Kay, Sequence determinants of compaction in intrinsically disordered proteins, Biophys. J. 98 (10) (2010) 2383–2390.
[86] S. Rodríguez-Enríquez, A. Marín-Hernández, J.C. Gallardo-Pérez, R. Moreno-Sánchez, Kinetics of transport and phosphorylation of glucose in cancer cells, J. Cell. Physiol. 221 (3) (2009) 552–559.
[87] A.P.P. Kröger, M.I. Komil, N.M. Hamelmann, A. Juan, M.H. Stenzel, J.M. J. Paulusse, Glucose single-chain polymer nanoparticles for cellular targeting, ACS Macro Lett. 8 (1) (2019) 95–101.
[88] M. Patra, S.G. Awuah, S.J. Lippard, Chemical approach to positional isomers of glucose–platinum conjugates reveals specific cancer targeting through glucose-transporter-mediated uptake in vitro and in vivo, J. Am. Chem. Soc. 138 (38) (2016) 12541–12551.
[89] C.S. Mahon, C.J. McGurk, S.M.D. Watson, M.A. Fascione, C. Sakonsinsiri, W. B. Turnbull, D.A. Fulton, Molecular recognition-mediated transformation of single-chain polymer nanoparticles into crosslinked polymer films, Angew. Chem. Int. Ed. 56 (42) (2017) 12913–12918.
[90] D.N.F. Bajj, M.V. Tran, H.-Y. Tsai, H. Kim, N.R. Paisley, W.R. Algar, Z.M. Hudson, Fluorescent heterotelechelic single-chain polymer nanoparticles: synthesis, spectroscopy, and cellular imaging, ACS Appl. Nano Mater. 2 (2) (2019) 898–909.
[91] L. Woythe, N.B. Tito, L. Albertazzi, A quantitative view on multivalent nanomedicine targeting, Adv. Drug Deliv. Rev. 169 (2021) 1–21.
[92] D. Pozzi, V. Colapicchioni, G. Caracciolo, S. Piovesana, A.L. Capriotti, S. Palchetti, S. De Grossi, A. Riccioli, H. Amenitsch, A. Laganà, Effect of polyethyleneglycol (PEG) chain length on the bio–nano-interactions between PEGylated lipid nanoparticles and biological fluids: from nanostructure to uptake in cancer cells, Nanoscale 6 (5) (2014) 2782–2792.
[93] L.M.P. Vermeulen, S.C. De Smedt, K. Remaut, K. Braeckmans, The proton sponge hypothesis: fable or fact? Eur. J. Pharm. Biopharm. 129 (2018) 184–190.
[94] S. Wijker, L. Deng, F. Eisenreich, I.K. Voets, A.R.A. Palmans, En route to stabilized compact conformations of single-chain polymeric nanoparticles in complex media, Macromolecules 55 (14) (2022) 6220–6230.

[95] I. Asenjo-Sanz, M. Del-Corte, J. Pinacho-Olaciregui, M. González-Burgos, E. González, E. Verde-Sesto, A. Arbe, J. Colmenero, J.A. Pomposo, Preparation and preliminary evaluation of povidone single-chain nanoparticles as potential drug delivery nanocarriers, Med One 4 (4) (2019), e190013.
[96] A. Sanchez-Sanchez, S. Akbari, A.J. Moreno, F.L. Verso, A. Arbe, J. Colmenero, J. A. Pomposo, Design and preparation of single-chain nanocarriers mimicking disordered proteins for combined delivery of dermal bioactive cargos, Macromol. Rapid Commun. 34 (21) (2013) 1681–1686.
[97] N.M. Hamelmann, S. Uijttewaal, S.D. Hujaya, J.M.J. Paulusse, Enhancing cellular internalization of single-chain polymer nanoparticles via polyplex formation, Biomacromolecules 23 (12) (2022) 5036–5042.
[98] N.M. Hamelmann, J.-W.D. Paats, Y. Avalos-Padilla, E. Lantero, L. Spanos, I. Siden-Kiamos, X. Fernàndez-Busquets, J.M.J. Paulusse, Single-chain polymer nanoparticles targeting the Ookinete stage of malaria parasites, ACS Infect. Dis. (2022), https://doi.org/10.1021/acsinfecdis.2c00336.
[99] D. Das, S. Srinivasan, A.M. Kelly, D.Y. Chiu, B.K. Daugherty, D.M. Ratner, P. S. Stayton, A.J. Convertine, RAFT polymerization of ciprofloxacin prodrug monomers for the controlled intracellular delivery of antibiotics, Polym. Chem. 7 (4) (2016) 826–837.
[100] D. Das, J. Chen, S. Srinivasan, A.M. Kelly, B. Lee, H.-N. Son, F. Radella, T.E. West, D.M. Ratner, A.J. Convertine, S.J. Skerrett, P.S. Stayton, Synthetic macromolecular antibiotic platform for inhalable therapy against aerosolized intracellular alveolar infections, Mol. Pharm. 14 (6) (2017) 1988–1997.
[101] E. Limqueco, D. Passos Da Silva, C. Reichhardt, F.-Y. Su, D. Das, J. Chen, S. Srinivasan, A. Convertine, S.J. Skerrett, M.R. Parsek, P.S. Stayton, D.M. Ratner, Mannose conjugated polymer targeting *P. aeruginosa* biofilms, ACS Infect. Dis. 6 (11) (2020) 2866–2871.
[102] S.J. Lam, E.H.H. Wong, C. Boyer, G.G. Qiao, Antimicrobial polymeric nanoparticles, Prog. Polym. Sci. 76 (2018) 40–64.
[103] K. Kuroda, G.A. Caputo, Antimicrobial polymers as synthetic mimics of host-defense peptides, WIREs Nanomed. Nanobiotechnol. 5 (1) (2013) 49–66.
[104] Y. Bai, X. Feng, H. Xing, Y. Xu, B.K. Kim, N. Baig, T. Zhou, A.A. Gewirth, Y. Lu, E. Oldfield, S.C. Zimmerman, A highly efficient single-chain metal–organic nanoparticle catalyst for alkyne–azide "click" reactions in water and in cells, J. Am. Chem. Soc. 138 (35) (2016) 11077–11080.
[105] C. Falciani, F. Zevolini, J. Brunetti, G. Riolo, R. Gracia, M. Marradi, I. Loinaz, C. Ziemann, U. Cossío, J. Llop, L. Bracci, A. Pini, Antimicrobial peptide-loaded nanoparticles as inhalation therapy for *Pseudomonas aeruginosa* infections, Int. J. Nanomedicine 15 (2020) 1117–1128.
[106] S. Ejaz, A. Ihsan, T. Noor, S. Shabbir, M. Imran, Mannose functionalized chitosan nanosystems for enhanced antimicrobial activity against multidrug resistant pathogens, Polym. Test. 91 (2020), 106814.
[107] R. Gracia, M. Marradi, U. Cossío, A. Benito, A. Pérez-San Vicente, V. Gómez-Vallejo, H.J. Grande, J. Llop, I. Loinaz, Synthesis and functionalization of dextran-based single-chain nanoparticles in aqueous media, J. Mater. Chem. B 5 (6) (2017) 1143–1147.
[108] C.T. Adkins, J.N. Dobish, S. Brown, E. Harth, Water-soluble semiconducting nanoparticles for imaging, ACS Macro Lett. 2 (8) (2013) 710–714.
[109] R. Liu, S. Liu, G. Hu, J.S. Lindsey, Aqueous solubilization of hydrophobic tetrapyrrole macrocycles by attachment to an amphiphilic single-chain nanoparticle (SCNP), New J. Chem. 44 (48) (2020) 21293–21308.
[110] S. Liu, J. Rong, R. Liu, J.S. Lindsey, Single-fluorophore single-chain nanoparticle undergoes fluorophore-driven assembly with fluorescence features retained in physiological milieu, ACS Appl. Polym. Mater. 3 (4) (2021) 1767–1776.
[111] Y. Li, Y. Bai, N. Zheng, Y. Liu, G.A. Vincil, B.J. Pedretti, J. Cheng, S. C. Zimmerman, Crosslinked dendronized polyols as a general approach to brighter and more stable fluorophores, Chem. Commun. 52 (19) (2016) 3781–3784.
[112] Z. Lu, J. Zhang, W. Yin, C. Guo, M. Lang, Preparation of AIE functional single-chain polymer nanoparticles and their application in H2O2 detection through intermolecular heavy-atom effect, Macromol. Rapid Commun. 43 (2022) 2200156.
[113] A. Blazquez-Martín, E. Verde-Sesto, A.J. Moreno, A. Arbe, J. Colmenero, J. A. Pomposo, Advances in the multi-orthogonal folding of single polymer chains into single-chain nanoparticles, Polymers 13 (2) (2021) 293.
[114] J.P. Cole, A.M. Hanlon, K.J. Rodriguez, E.B. Berda, Protein-like structure and activity in synthetic polymers, J. Polym. Sci. A Polym. Chem. 55 (2) (2017) 191–206.
[115] W. Wen, T. Huang, S. Guan, Y. Zhao, A. Chen, Self-assembly of single chain Janus nanoparticles with tunable liquid crystalline properties from stilbene-containing block copolymers, Macromolecules 52 (8) (2019) 2956–2964.
[116] S. Kaga, N.P. Truong, L. Esser, D. Senyschyn, A. Sanyal, R. Sanyal, J.F. Quinn, T. P. Davis, L.M. Kaminskas, M.R. Whittaker, Influence of size and shape on the biodistribution of nanoparticles prepared by polymerization-induced self-assembly, Biomacromolecules 18 (12) (2017) 3963–3970.
[117] X. Xie, J. Liao, X. Shao, Q. Li, Y. Lin, The effect of shape on cellular uptake of gold nanoparticles in the forms of stars, rods, and triangles, Sci. Rep. 7 (1) (2017) 3827.
[118] P. Malo de Molina, T.P. Le, A. Iturrospe, U. Gasser, A. Arbe, J. Colmenero, J. A. Pomposo, Neat protein single-chain nanoparticles from partially denatured BSA, ACS Omega 7 (46) (2022) 42163–42169.
[119] K. Korschelt, M.N. Tahir, W. Tremel, A step into the future: applications of nanoparticle enzyme mimics, Chem. Eur. J. 24 (39) (2018) 9703–9713.
[120] R. Ragg, F. Natalio, M.N. Tahir, H. Janssen, A. Kashyap, D. Strand, S. Strand, W. Tremel, Molybdenum trioxide nanoparticles with intrinsic sulfite oxidase activity, ACS Nano 8 (5) (2014) 5182–5189.
[121] L. Alili, M. Sack, C. von Montfort, S. Giri, S. Das, K.S. Carroll, K. Zanger, S. Seal, P. Brenneisen, Downregulation of tumor growth and invasion by redox-active nanoparticles, Antioxid. Redox Signal. 19 (8) (2013) 765–778.
[122] D. Zhang, Y.-X. Zhao, Y.-J. Gao, F.-P. Gao, Y.-S. Fan, X.-J. Li, Z.-Y. Duan, H. Wang, Anti-bacterial and in vivo tumor treatment by reactive oxygen species generated by magnetic nanoparticles, J. Mater. Chem. B 1 (38) (2013) 5100–5107.